Marine and Petroleum Geology 138 (2022) 105574

Contents lists available at ScienceDirect

Marine and Petroleum Geology

journal homepage: www.elsevier.com/locate/marpetgeo

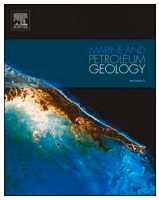

Early deformation structures connected to the progradation of a carbonate platform: The case of the Nuvolau Cassian platform (Dolomites - Italy)

Niccolò Menegoni [a,*], Riccardo Inama [b], Matteo Crozi [a], Cesare Perotti [a]

[a] Department of Earth and Environmental Sciences, University of Pavia, Via Adolfo Ferrata 4, Pavia, 27100, Italy
[b] SIGNAL. s.r.l, Via Fratelli Cuzio 42, Pavia, 27100, Italy

A B S T R A C T

Among the several Triassic carbonate platforms of the Dolomites, the high and vertical cliff of the Gusela del Nuvolau Cassian carbonate platform provides one of the best exposures of a platform - basin transition. However, its analysis using traditional filed surveys can often be limited and distorted due to the difficult and often impossible accessibility of its walls and the lack of optimal observation points. For this reason, in this study an analysis based on the Digital Outcrop Model (DOM) developed by Uncrafted Aerial Vehicle (UAV) digital photogrammetry technique was used. The 3D DOM analysis allowed to properly determine the stratal geometry and the fracture network of the carbonate platform and underlying basinal deposits (San Cassiano Formation) and to identify the presence of early deformation structures. These structures were probably driven by the differential compaction of the basinal facies that is due the differential load of the carbonate platform as confirmed by the numerical 2D models. These structures are generally orthogonal to the NE progradation direction of the carbonate platform, as in the nearby Lastoni di Formin platform.

1. Introduction

Between 50% and 60% of the world's hydrocarbon reserves are held in carbonate reservoirs. The Middle East, for example, is characterized by large carbonate fields that host around 70% of oil and 90% of gas reserves (Beydoun, 1986; Nairn and Alsharhan, 1997). Moreover, carbonate aquifers are probably one of the most important thermal water resources outside of volcanic areas (Goldscheider et al., 2010).

The porosity and permeability of carbonate reservoirs are often secondary as are due to fracturing and in some reservoir rocks such as low-porosity carbonates, secondary permeability provides the main flow conduit for fluid migration. The presence in carbonate reservoirs of fracture corridors with an extent of hundreds of meters in width and height and an area in the order of kilometers represent primary pathways for hydrocarbon migration. Generally, these structures have a permeability incomparably greater than the rock matrix, having a considerable influence on hydrocarbon and water production and recovery (Nelson, 2001).

In recent years, the role of syn-depositional fractures in controlling the permeability and flow of fluids in carbonate bodies has been progressively recognized of crucial importance. Early fractures are often characterized by a great aperture and non-matching margins (Inama, 2020) and generally they are subjected to repeated mobilizations under the action of subsequent tectonic stress fields. These peculiar features make them the principal hydraulic patways of the carbonate reservoirs, enhancing permeability (Koša and Hunt, 2005; Frost and Kerans, 2009; Berra and Carminati, 2012), providing pathways for fluid flow and playing a significant role in the migration of early diagenetic fluids, triggering karst development.

A connection between the dynamic of a carbonate platform and its early fracturing has been already hypothesized (Frost and Kerans, 2009; Berra and Carminati, 2012; Budd et al., 2013; Ibrayev et al., 2016; Nooitgedacht et al., 2018; Nolting et al., 2020), however only few study investigated the mechanisms with which fractures develop during platform evolution (e.g. Nolting et al., 2020).

The eastern sector of the Gusela del Nuvolau Cassian carbonate platform (Upper Ladinian – Lower Carnian age) provides one of the best exposures of the platform-to-basinal transition and the geometrical connection between slope and basinal deposits (the heteropic San Cassiano Formation) (Bosellini, 1984; Blendinger and Blendinger, 1989), where the relationships between early fractures and the progradation of a platform can be observed and measured. However, the geological and structural analysis is locally very difficult due to the huge dimensions and inaccessibility of the outcrops (sub-vertical cliffs), and also distant observations are often affected by perspective errors caused by unfavorable exposure of the outcropping cliffs (e.g. the absence of outcrops

* Corresponding author.
E-mail addresses: niccolo.menegoni@unipv.it (N. Menegoni), inama@signalitalia.com (R. Inama), matteo.crozi@unipv.it (M. Crozi), cesare.perotti@unipv.it (C. Perotti).

https://doi.org/10.1016/j.marpetgeo.2022.105574
Received 20 November 2021; Received in revised form 14 January 2022; Accepted 1 February 2022
Available online 4 February 2022

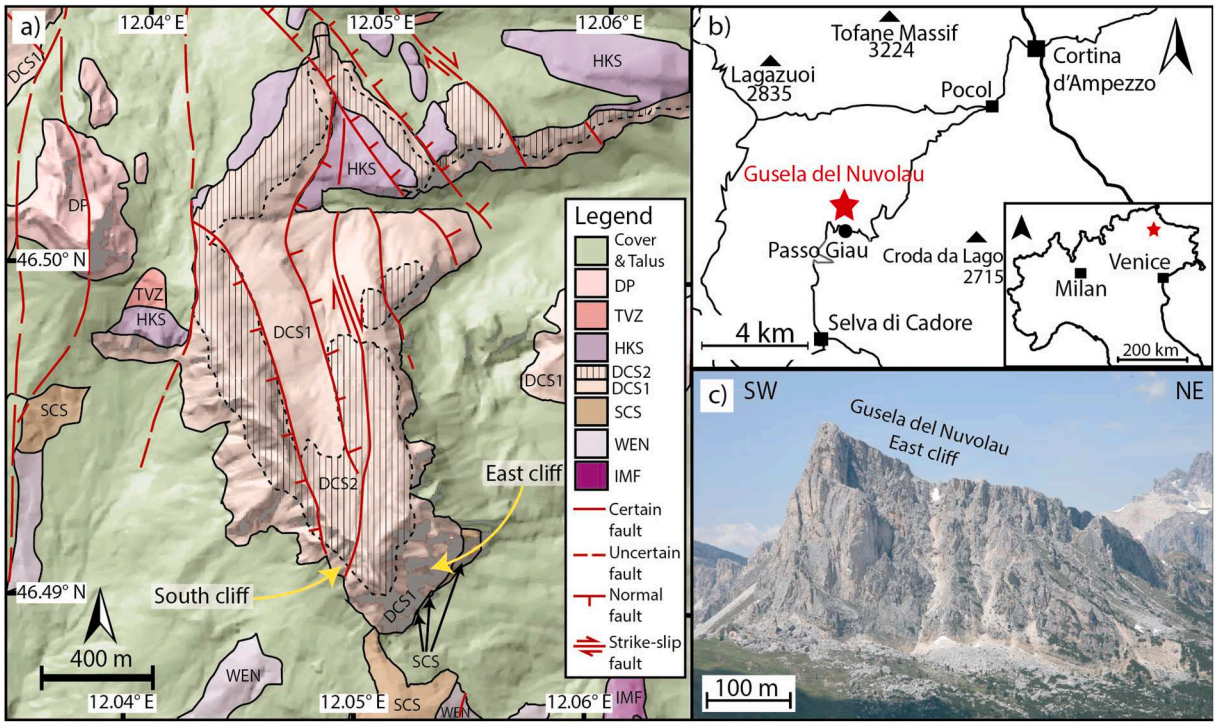

Fig. 1. (a) Geological map of the Gusela del Nuvolau surrounding area (from Neri et al., 2007, modified), (b) location map of the outcrop, and (c) terrestrial panoramic view of the Gusela del Nuvolau. DP, Dolomia Principale; TVZ, Travenanzes Fm.; HKS, Heiligkreuz Fm.; DCS, Cassian Dolomite (differentiated in DSC1 and DSC2 according to Neri et al., 2007); SCS, San Cassiano Fm.; WEN, Wengen Fm.; SCI, Sciliar Fm.; IMF, Mt. Fernazza Fm.

exactly perpendicular to the direction of progradation) and occlusions that can lead to significant errors in the interpretation of the outcrop geometries.

For all these reasons the geological study of the platform was conducted by the analysis of detailed photogrammetric Digital Outcrop Models (DOMs) that were realized using Unmanned Aerial Vehicles (UAV or drones) and Structure from Motion (SfM) process. This technique allowed to acquire quantitative information along the vertical and inaccessible cliffs of the Gusela del Nuvolau, and to study the outcropping structures. Digital photogrammetry is an important source of data in many fields of geosciences (Hodgetts et al., 2004; Casini et al., 2016; Cawood et al., 2017; Corradetti et al., 2017; Burnham and Hodgetts, 2019; Menegoni et al., 2019; Inama et al., 2020) because it allows the reconstruction of georeferenced 3D outcrop models that can be visually analyzed in a stereoscopic environment with high-resolution images and without perspective distortion, and where accurate measurements of structures of every size can be acquired.

The use of UAVs allows shooting remote or inaccessible portions of the outcrops (Sturzenegger and Stead, 2009; Menegoni et al., 2018; Inama et al., 2020), reducing occlusions and vertical orientation biases. In addition, the processing of high-resolution DOMs can produce orthorectified images collected from different points of view (Gattolin et al., 2015; Tavani et al., 2016; Corradetti et al., 2017; Inama et al., 2020).

2. Geological setting

The *Gusela del Nuvolau* is an isolated peak that outcrops in a dominant position a few hundred meters north of Passo Giau (Belluno province, Italy) and is one of the major elevations of the Nuvolau Group, in the central-eastern Italian Dolomites (Fig. 1).

The Dolomites are part of the Southern Alpine domain and are bounded to the north by the Funes-Passo delle Erbe line and to the south by the south verging Valsugana thrust (Doglioni, 1987). During the Alpine orogeny, most of the strain was accommodated by intensive thrusting at the southern margin of the Alps, and the central part of the chain was only mildly deformed by tectonics (Bosellini and Neri, 1991; Mollema and Antonellini, 1999), preserving the seismic-scale depositional geometries of the Middle Triassic platforms.

The outcrop of *Gusela del Nuvolau* represents the remnants of an exhumed Cassian buildup of Upper Ladinian – Lower Carnian age (Fig. 2).

This generation of platforms (Cassian Dolomite, Neri et al., 2007), belonging to the so called post-volcanic platforms, are dominated by prograding slope deposits and associated with shallowing basinal succession (Stefani et al., 2010).

Several authors (Leonardi, 1968; Bosellini et al., 1982; Blendinger and Blendinger, 1989) have pointed out that the Gusela was part of a larger carbonate platform extended approximately between Falzarego/Valparola and Giau passes, and including the outcrops of *Sass de Stria, Col Gallina* and *Averau* to west and the *Lastoni di Formin* to east. The lithology of the Cassian Dolomite consists of greyish and whitish fine grained dolostone with sucrose texture. The dolomitization of the Cassian platform is often pervasive and the original texture of the rock, the fossil content and the sedimentary structures are hardly recognizable: the reconstruction of the biota is largely based on studies of isolated and undolomitized olistholites (cipit boulders), and swarms of carbonate material embedded in the coeval basinal sediments of the San Cassiano Formation (Russo et al., 1997).

The eastern wall of the *Gusela* represents a spectacular example of the platform-to-basin transition: while the small topmost part of the mountain corresponds to the platform interior, the outcrop is mainly constituted by the massive northward-dipping clinoforms of the slope facies, that prograded over the coeval basinal deposits, composed by marly limestones (San Cassiano Formation). The exceptional exposure of the depositional geometries gives the opportunity to study in detail the processes that control the progradation of the Cassian Dolomite platform.

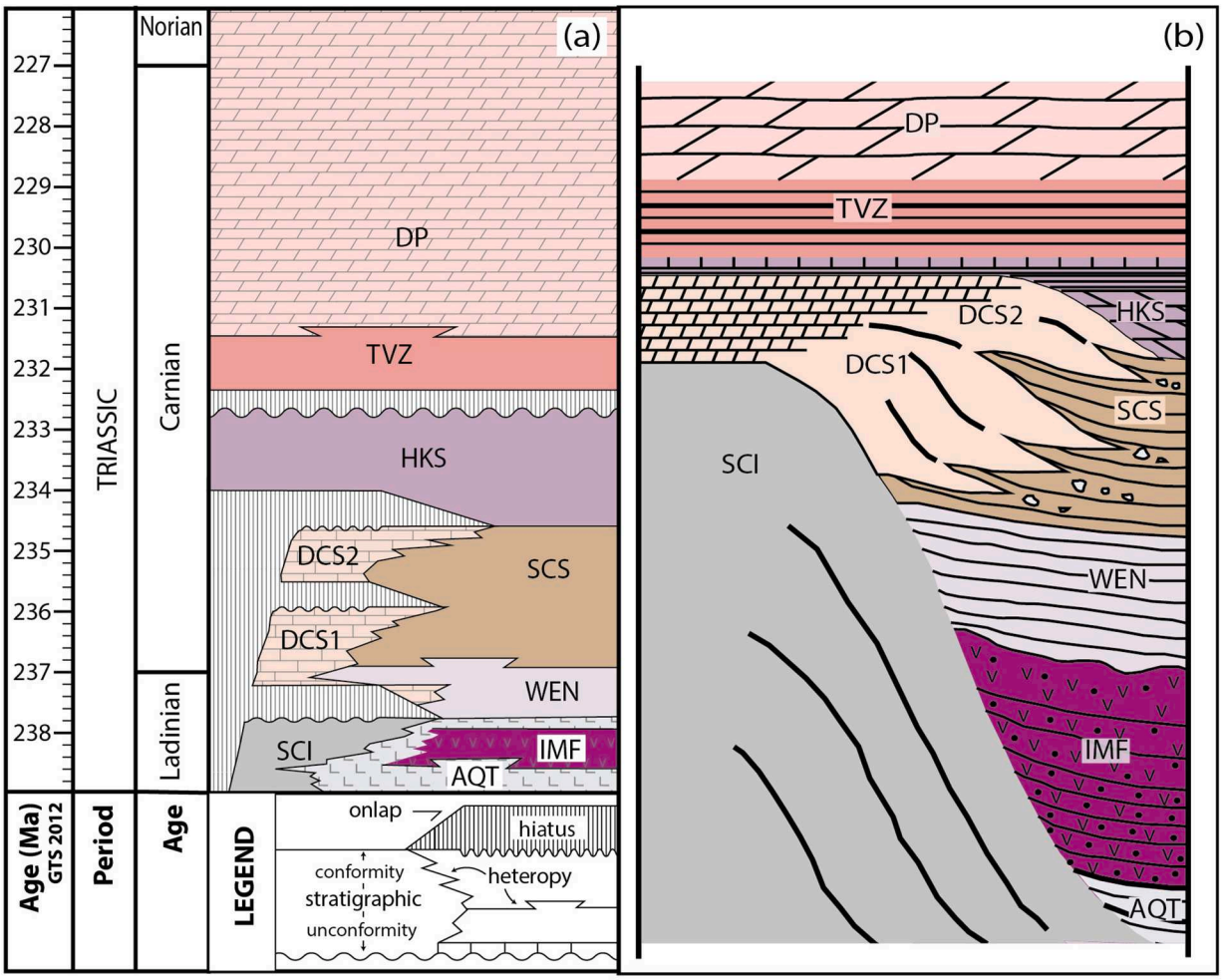

Fig. 2. (a) Stratigraphic framework of part of Middle and Upper Triassic of the central-eastern Dolomites (from Preto et al., 2017, redrawn) and (b) simplified sketch of the stratigraphic relationships in the study area (modified after Neri et al., 2007 and Inama et al., 2020). DP, Dolomia Principale; TVZ, Travenanzes Fm.; HKS, Heiligkreuz Fm.; DCS, Cassian Dolomite (differentiated in DSC1 and DSC2 according to Neri et al., 2007); SCS, San Cassiano Fm.; WEN, Wengen Fm.; SCI, Sciliar Fm.; IMF, Mt. Fernazza Fm.; AQT:Acquatona Fm.; LVN: Livinallongo Fm.

2.1. Tectonic history and structural evolution

From Mesozoic Dolomites underwent a complex tectonic evolution. During Late Permian – Early Triassic, a rifting phase generated two principal N–S trending structural highs and lows (Doglioni, 1987; Bosellini et al., 2003) allowing the development of the so called Trento platform and the Carnico-Bellunese basin. During Ladinian, a local sinistral transpressive tectonic induced the development of flower structures and high angle strike slip faults concentrated along the alignment of the Strava fault and Cima Bocche anticline, characterized by a N70° direction (Doglioni, 1987). The age of these structures was determined by the cross-cutting relationships with the Late Ladinian - Early Carnian volcanic and plutonic bodies related to the emplacement of the intrusive complexes of Predazzo and Monzoni (Doglioni, 1987; Castellarin., 1988; Abbas et al., 2018).

From Late Trassic to Jurassic times the Dolomites were subjected to a rifting process and progressively became part of the passive continental margin of the Adria plate (Bertotti, 2001; Berra and Carminati, 2012). Due to the rifting, the Dolomia Principale platform was fragmented in different structural highs and lows characterized by the presence of N–S striking normal faults (Doglioni, 1987). During Paleogene and Neogene Alpine tectonics, the Dolomites became the innermost part of a south-verging thrust belt (Doglioni, 1987; Berra and Carminati, 2012). Extensive investigations show as the Alpine compressional tectonics is outlined by different phases (Caputo, 1996; Caputo et al., 1999, 2010). In the Dinaric phase (Chattian-Burdigalian) the maximum compressive axis was oriented ENE-WSW (Caputo, 1996, 2008). Between Serravallian and Tortonian (Alpine - Valsuganense phase) N–S to NW-SE compression was recorded by the orientation of the major overthrusts (i.e., Valsugana and Belluno overthrusts, Doglioni, 1987; Antonellini and Mollema, 2000; Caputo, 1996; Schönborn, 1999). In the Late Messinian–Pliocene times, the last Alpine phase (Schledrense phase) was characterized by the reorientation of the maximum compression axis to NW-SE (Caputo, 1996; Castellarin et al., 1992), depicting an anticlockwise rotation of the main compressive direction from NE-SW to NW-SE (Caputo, 1996; Mazzoli and Helman, 1994).

Despite this long tectonic history, Dolomites are only slightly deformed in a large pop-up syncline of Neogene age (Doglioni and Castellarin, 1985; Doglioni, 1987; Castellarin et al., 1992; Bosellini et al., 2003) and exhibit several generations of different and well-exposed Triassic carbonate platforms.

3. Geometry of clinoforms

Some of the Middle - Triassic carbonate platforms outcropping in the Dolomites are characterized by the superb exposure of the platform-to-basin transition (i.e. Sella, Rosengarten) and the extraordinary preservation of the slope facies geometries. The several generations of platforms that developed from Anisian to Carnian display different evolution and geometries (controlled by the progradation to

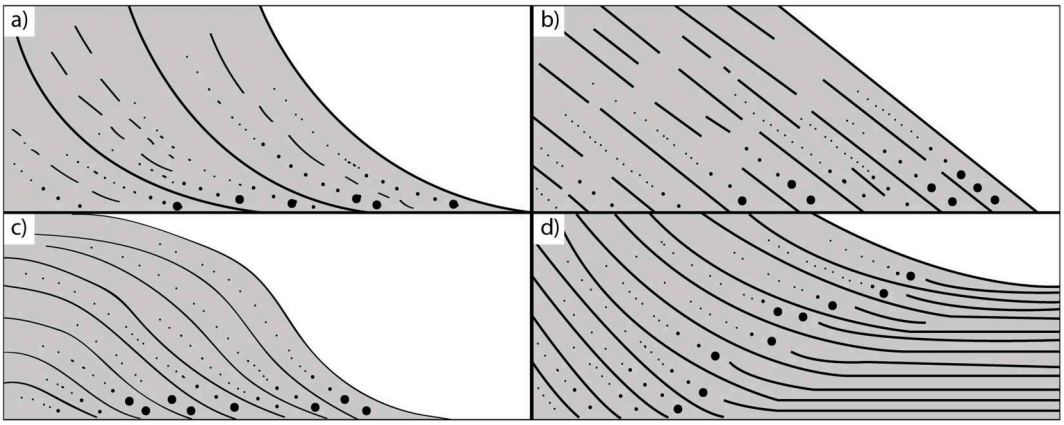

Fig. 3. The four main geometrical configurations of clinoforms, depicted by Bosellini (1984), as a function of sediment fabric and distribution along the slope: (a) oblique-tangent pattern, (b) oblique-parallel pattern, (c) sigmoidal-oblique pattern and (d) flattening-out pattern (redrawn from Bosellini, 1984).

aggradation ratio) and slope angles. Growth and architecture of carbonate platforms are controlled by several sedimentary, biological and physical factors (Schlager, 1993; Maurer, 2000; Marangon et al., 2011; Preto et al., 2017; Reijmer, 2021), and a certain degree of variability in terms of depositional geometries is also possible within platforms of the same age.

The Anisian Contrin platforms show thickness that normally ranges between 50 and 150 m (occasionally 500 m) flanked by large clinostratified (15–20°) slope bodies. Anisian platforms aggraded very fast in response to extremely high subsidence values (Gianolla et al., 2008; Preto et al., 2011). The subsidence ratio was estimated around 600–1500 m/Myr (Franceschi et al., 2020), while the platforms reached 700–800 m of thickness (e.g. Rosengarten, Marmolada and Latemar platforms) and developed slopes with different geometry (Stefani et al., 2010; Gianolla et al., 2021). Slopes are generally characterized by a concave upward shape with inclination of 10°–25° in the early phase, and a very steep planar morphology (30° – 42°) in the late pre-volcanic phase. During the early Ladinian subsidence decreased to negligible values and the carbonate platforms expanded by progradation for several km over the adjacent basins producing large clinostratified slope breccia bodies (Maurer, 2000, Bosellini et al., 2003). The Carnian generation of buildups (Cassian Dolomite) displays clinostratified slope angles that reach 20°–30° (Bosellini et al., 2003) that progressively decrease at the toe of slope (Keim et al., 2001). However, slope angles can vary depending on the carbonate factory that supplies the sediment and the processes operating on the slopes (Kenter, 1990; Keim and Schlager, 1999, 2001; Trombetta, 2011).

Few studies carried out in the Dolomites described the variability of clinoforms shape (e.g. Bosellini, 1984; Kenter, 1990; Adams and Schalger, 2000). In particular, Bosellini (1984) describes four main geometrical configurations of clinoforms as a function of sediment fabric and distribution along the slope: (a) oblique-tangent pattern, (b) oblique parallel pattern, (c) sigmoidal-pattern and (d) flattening-out pattern (Fig. 3).

The oblique-parallel pattern forms where the slope beds are composed of coarse talus debris (e.g. megabreccia) that can deposit with a relatively high angle of repose at the footslope, as the case of the Catinaccio; the other geometries occur where the deposits have lower grain size (gravel, sand, mud), as for Gusela de Nuvolau and western and southern Sella. Notwithstanding, according to Bosellini (1984) the flattening-out geometry (configuration c) could be strongly influenced by the slope height (lower height, stronger flattening-out geometry). The oblique-parallel clinoforms, also called planar clinoforms, are characterized by "a homogeneous foreslope and often exhibit abrupt or sub-horizontal downlap patterns" (Playton et al., 2010). The shape of oblique tangential and flattening-out clinoforms, also called exponential clinoforms, is influenced by the gradational facies changes and basinward fining along dip (Playton et al., 2010). The Sella platform represents a key example of the mutual relationship between basinal sedimentation and platform progradation rates. The southward and westward clinoforms, facing the major volcanoclastic source, shows climbing progradation, while the slope in the northern side of the platform displays a quasi-horizontal contact between clinoforms and basinal deposits: this is probably caused by a reduced sediment supply due to the barrier formed by the platform itself for sediments carried from south (Bosellini et al., 1982; Bosellini, 1984; Doglioni, 1987).

Table 1
Specification of the UAV used to perform the Digital Photogrammetric survey.

Type	DJI Phantom 4 RTK	DJI Mavic Air 2
Weight (payload included)	1391 g	570 g
Camera sensor size	1 inch	1/2 inch
Camera sensor resolution	20 megapixels	48 megapixels
GNSS type	Professional (Real Time Kinematic)	Consumer (standalone)
GNSS accuracy	<5 cm	>2 m

4. Methodology

The facies and geometry analysis of the Gusela del Nuvolau platform are hampered by its unfavorable exposure, huge dimensions, and extremely difficult access to the outcrops (e.g. sub-vertical cliffs inspectable only by climbing with a high hazard of rockfall). Also the extensive dolomitization often partially obliterates the original depositional fabric, the sedimentary structures and the fossil content, similarly to the nearby Lastoni di Formin outcrop (Inama et al., 2020). For these reasons, the geological analysis of the Gusela del Nuvolau Platform was performed coupling the traditional field survey with the Uncrafted Aerial Vehicle (UAV)-based Digital Photogrammetry (DP). This technique permits overcoming the main limitation of the traditional field survey, such as the impossibility to reach the inaccessible position of the outcrops and properly visualize the geological structures from a correct point of view (Tavani et al., 2016; Inama et al., 2020).

4.1. UAV digital photogrammetry survey and Digital Outcrop Models development

The UAV Digital Photogrammetry survey (UAVDP) was achieved using two different types of quadcopters, one equipped with a standard Global Navigation Satellite System (GNSS) and another with a high accuracy Real Time Kinematic (RTK)-GNSS.

Table 2
Specification of the UAVs surveys.

UAV Type	DJI Phantom 4 RTK	DJI Mavic Air 2
Number of flights/models	6	4
Distance camera-outcrop range (m)	30–200	20–80
Image resolution range (cm)	1–5	0.3–1

The specifications of the two UAVs are reported in Table 1.

The main differences between the two drones regard the weight and the GNSS accuracy. The quadcopter DJI Phantom 4 RTK can record the position of image acquisition with higher accuracy (<5 cm), but it requires the positioning of the D-RTK2 GNSS-base station that can make the mission planning more complicated. For its lightweight and lower cost the quadcopter DJI Mavic Air 2 was used in a more 'carefree' way flying much closer to the outcrop, thereby acquiring pictures with a higher resolution.

For this reason, the DJI Phantom 4 RTK was used to acquire the images of the entire outcrop, whereas the DJI Mavic Air 2 was used to acquire images with a very-high resolution and, therefore, to cover with a high resolution some details of the outcrop.

The specifications of the UAV-DP surveys conducted by the two drones are reported in Table 2.

The images acquired by the UAVs were then used to elaborate the Digital Outcrop Models. The DOMs were developed using the Metashape software (Agisoft, 2019) processing the image at the full resolution, following the procedures described in Inama et al. (2020). The result of the DOMs development is shown in Figs. 4 and 5.

4.2. Digital Outcrop Models accuracy

Due to the use of a UAV with RTK-GNSS, a Ground Control Points (GCPs) survey was not performed. Several studies (Peppa et al., 2019; Taddia et al., 2019, 2020; Stott et al., 2020; Štroner et al., 2020) show that using the quadcopter DJI Phantom 4 RTK, together with the D-RTK2 GNSS base station, it is possible to obtain absolute accuracies lower than 7 cm that is considered largely sufficient for the aims of this study.

The DOMs obtained using the DJI Mavic Air 2 quadcopter that is equipped with a low-cost GNSS were elaborated using the positions registered by the onboard GNSS and, then, they were appropriately translated to fit the high-precision models developed using the DJI Phantom 4 RTK quadcopter. These translations are in general about 2–5 m and correspond to the absolute accuracies of these models.

After the translation of the DOMs developed with the quadcopter DJI Mavic Air 2, the relative accuracy was estimated using the methodology described in Menegoni et al. (2019) and Inama et al. (2020), which consist in calculating the difference in scale and orientation of the vectors that join the real points of the world and those that join the equivalent points onto the models. The comparison of 45 vectors that join the points of the high-accuracy DOMs, developed with the DJI Phantom 4RTK, with the equivalent points of the DOMs developed with the DJI Mavic Air 2 indicate a difference in scale and orientation lower than 0.8° and 0.45%, respectively. These values indicate a good relative accuracy of the DOMs developed using the DJI Mavic Air 2 and are coherent with the values reported by Menegoni et al. (2019) and Inama et al. (2020) for DOMs developed using UAVs equipped with low-cost GNSS.

4.3. Digital Outcrop Models analysis

The analysis of the Digital Outcrop Models (DOMs) was conducted using the open-source CloudCompare software (CloudCompare, 2019) that permits visualization of the DOMs in a 3D-stereoscopic environment and collection of 3D measures with high precision (Menegoni et al., 2018; Inama et al., 2020). In particular, bedding, fractures and faults, together with their geometric information, as attitude, position and dimension were measured and mapped (Fig. 6). Whereas the 3D mapping of the bedding (3D line drawing) was performed mainly using the Compass plugin of CloudCompare (Thiele et al., 2017), the 3D mapping of the fractures and faults was done manually by picking the fractures

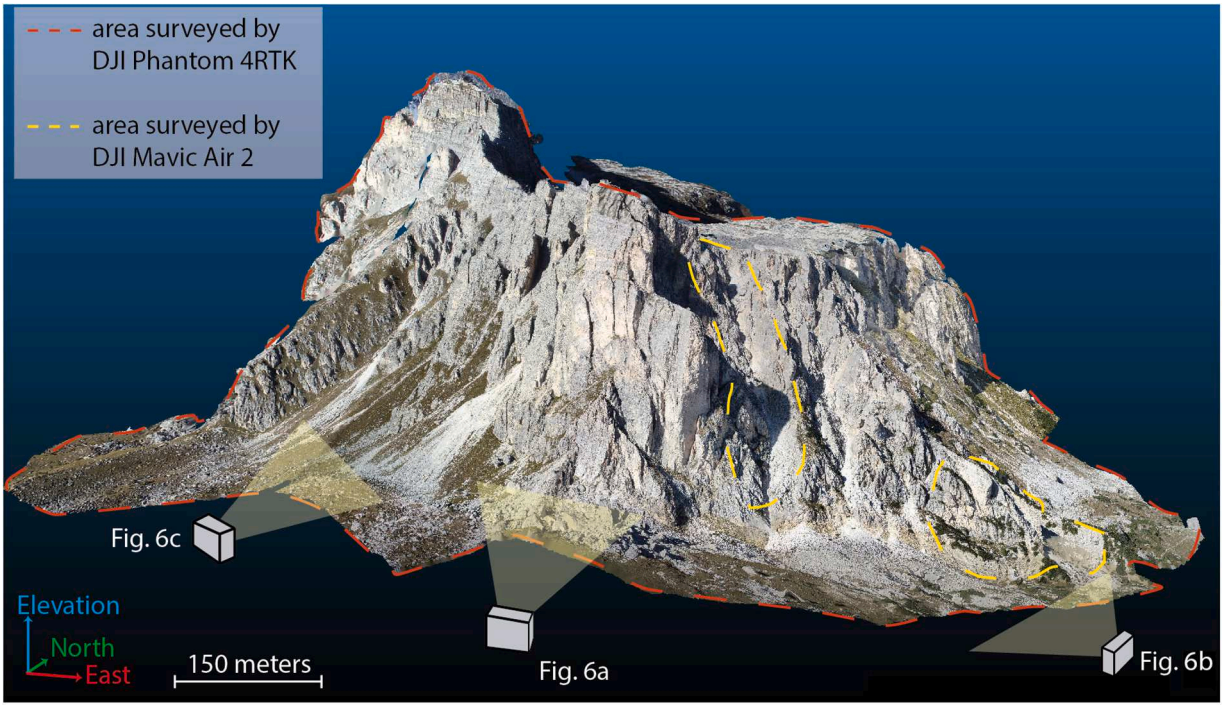

Fig. 4. 3D oblique view of the mosaic of all the Digital Outcrop Models (DOMs) developed using the images acquired by the UAVs. The red dashed line delimits the area covered by the DJI Phantom 4RTK surveys, whereas the yellow dashed lines delimit the areas covered by the DJI Mavic Air 2 surveys. The grey boxes represent the point of view of the next figures (Fig. 5a, b and 5c). (For interpretation of the references to colour in this figure legend, the reader is referred to the Web version of this article.)

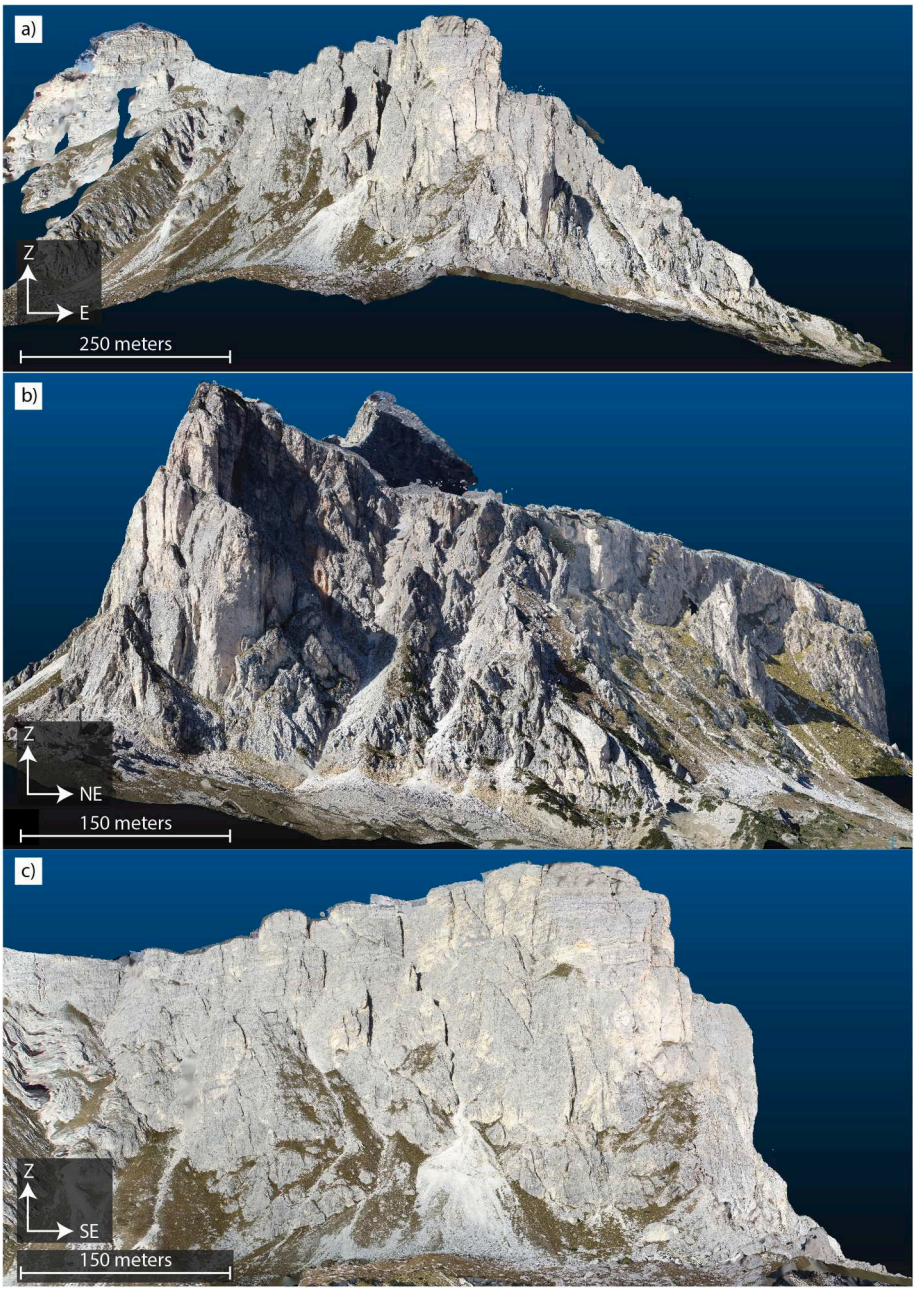

Fig. 5. The Digital Outcrop Models (DOMs) viewed from different horizontal views. (a) North-view of the Gusela del Nuvolau outcrop from the Passo Giau road, from where both the 'South cliff' and 'East cliff' are visible. (b) NW-view of the 'East cliff' which is roughly parallel to the N-NE progradation of the platform. (c) 'South cliff' of the Gusela del Nuvolau viewed from SW.

and faults points and interpolating the best-fit 3D plane.

5. Results

5.1. Analysis of the platform geometry and facies

The visual inspection and 3D interpretation of the developed DOM allowed us to identify the geometry and the sedimentological features of the 3 principal facies outcropping in the area, the inner platform beds, slope clinoforms and thinly layered basinal deposits (Fig. 7).

In the southwestern upper part of the outcrop, a succession of regular and well stratified beds was identified and interpreted as the inner platform facies of the Cassian Dolomite. The mean attitude and thickness of the recognized beds are around 028°N/25° (dip direction/dip; Figs. 8) and 2 m, respectively.

The inner platform beds increase their thickness moving towards the margin (Fig. 9).

The variation of the beds from the inner part of the platform toward its margin was calculated on the DOM measuring the real thickness of the selected packs of strata using the Compass plugin of CloudCompare (Thiele et al., 2017) (Fig. 10).

The analysis clearly shows that the strata increase their thickness moving toward the margin (Fig. 10b).

The clinoforms that represent the slope of the platform (marked by purple lines in Fig. 8b) show a higher attitude variability with respect to the inner platform beds; on average, they dip towards NE (036°N/35°) and have a variable thickness of about 5–10 m (Fig. 11).

The inclination of the clinoforms increases from the margin of the platform to the upper slope and decreases at the toe of the slope toward the slope-basin contact as confirmed also by the relationships between

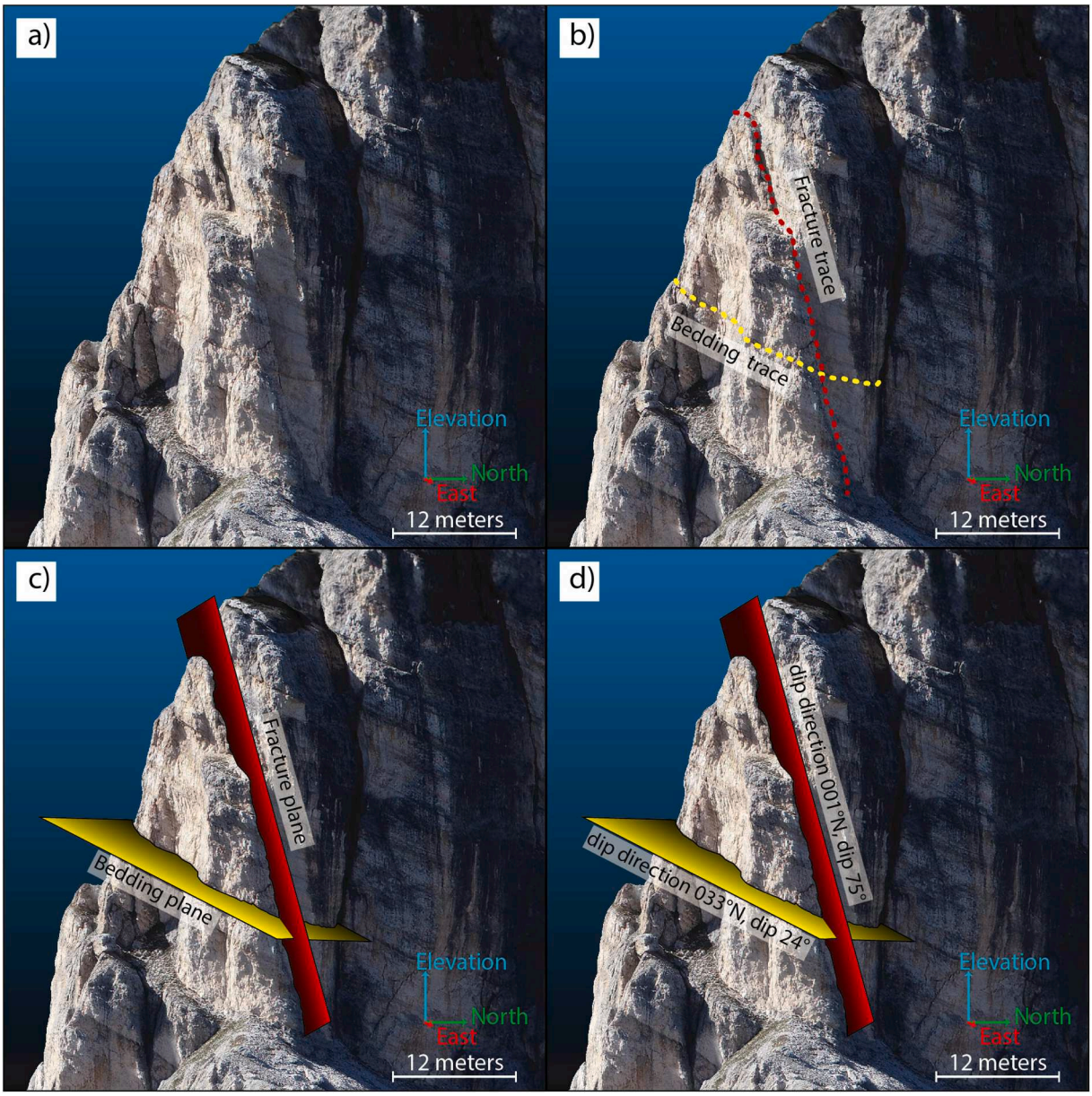

Fig. 6. Example of the workflow used for the 3D mapping of the geological features of the Digital Outcrop Model (DOM): (a) 3D inspection of the DOM; (b) bedding and fracture traces detection and mapping through semi-automatic tracing (Thiele et al., 2017) and manual point picking (Inama et al., 2020); (c) estimation of the 3D planes that best-fit the bedding and fracture traces; (d) calculation of the attitude of the bedding and fracture planes.

their dip angles and the altitude where the measurements are performed (Fig. 12).

Notwithstanding, due to the impossibility to identify continuous clinoforms from the platform margin to the basin, it was not possible to perform an accurate quantitative analysis of the dip variation along the slope.

In the basal part of the east-facing rock cliff, some limited successions of regular, well defined thin beds of the basinal facies of the San Cassiano Formation, were identified. The tabular and regular bedding surfaces recognized onto the DOM have a mean attitude and thickness of 029°N/25° and 20 cm, respectively (Fig. 13), as confirmed by measurements locally performed in the field.

In the study area, the San Cassiano formation consists of shales, marls and pelites alternating with volcanoclastic materials and gravity-displaced swarms of oolitic-bioclastic calcarenites (Fig. 14), derived from the upper part of the platforms (Fig. 15).

In some portions of the outcrop, close to the termination of the clinoforms, the basinal unit is affected by folds that are possibly related to faulting (Fig. 16) or compaction processes (Fig. 17). In general, the fold axes seem horizontal with a NW-SE direction.

The restoration of the original geometry of the Gusela del Nuvolau platform was obtained by bringing the inner platform strata back to the horizontal with a rotation around their direction with an angle equal to their average inclination (Fig. 18).

After the restoration, the mean dip direction of the clinoforms was 055°N suggesting a progradation of the platform towards N-E.

5.2. *Fracture network analysis*

The fracture network analysis of the Gusela del Nuvolau massif was performed by 2D and 3D mapping.

The 2D analysis was conducted using a zenithal orthoimage with a resolution of 30 cm, and a 1 m resolution airborne LiDAR-based DTM (data retrievable from *Geoportale Nazionale of Ministero dell'Ambiente e*

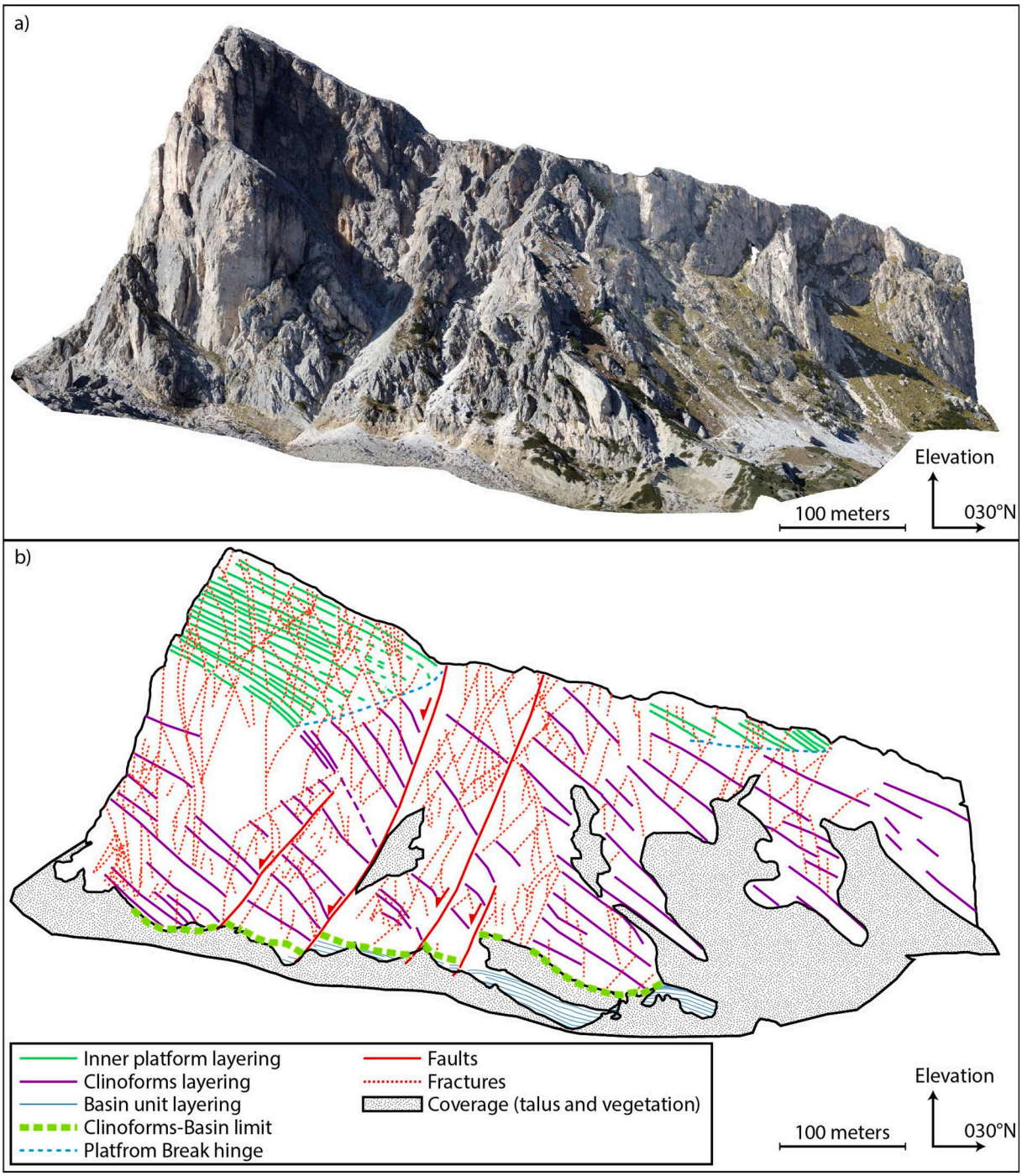

Fig. 7. (a) Orthographic view of the East cliff of the Gusela del Nuvolau DOM and (b) its interpretation; in the sketch only the main tectonic and stratigraphic surfaces are indicated.

della Tutela del Territorio e del Mare at http://www.pcn.minambiente.it/mattm/) by mapping all the visible fracture traces. The acquired 2D fracture dataset is composed of 152 fracture traces with a mean length of ca. 80 m and a minimum and a maximum length of 10 m and 579 m, respectively (Fig. 19).

The rose plot of the azimuth of the fracture traces (Fig. 20b) highlights the presence of 2 different fracture sets: K1 with an azimuth mode of 120°–130°N, and K2 with an azimuth mode of 150°–160°N. The direction of these two sets is very similar to those reported by Inama et al. (2020) for the Lastoni di Formin outcrop.

Moreover, 339 faults and fractures with their attitudes were detected by the 3D analysis of the DOM that was performed onto the 'south' and 'east' cliffs of the outcrop (Fig. 20).

The fracture dataset was discriminated in (i) faults (fractures with a visible displacement) and major fracture and (ii) minor fractures. Major fractures are considered the fractures that cut the whole outcrop (generally with a dimension greater than 100 m), while minor fractures have a dimension lower than 100 m. Faults and major fractures affect the entire outcrop, while minor fractures are located principally in the inner platform.

Both the 3D fracture data show the presence of 3 main sets:

- K1, the most abundant set with a sub-vertical and NW-trending attitude;

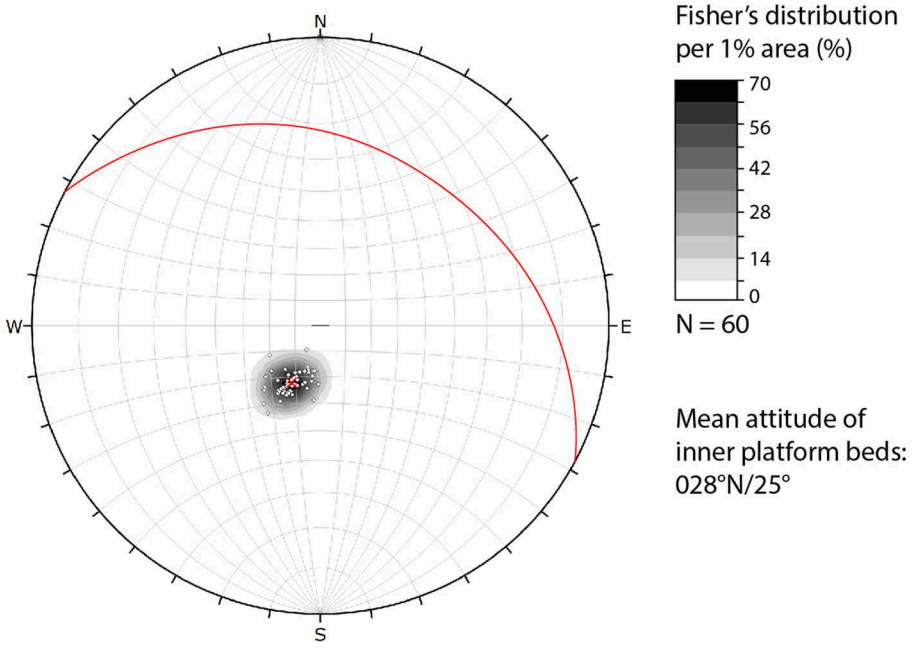

Fig. 8. Contour of the poles of the inner platform beds. The red line and cross mark the mean plane and pole, respectively (lower hemisphere and equal angle projection). (For interpretation of the references to colour in this figure legend, the reader is referred to the Web version of this article.)

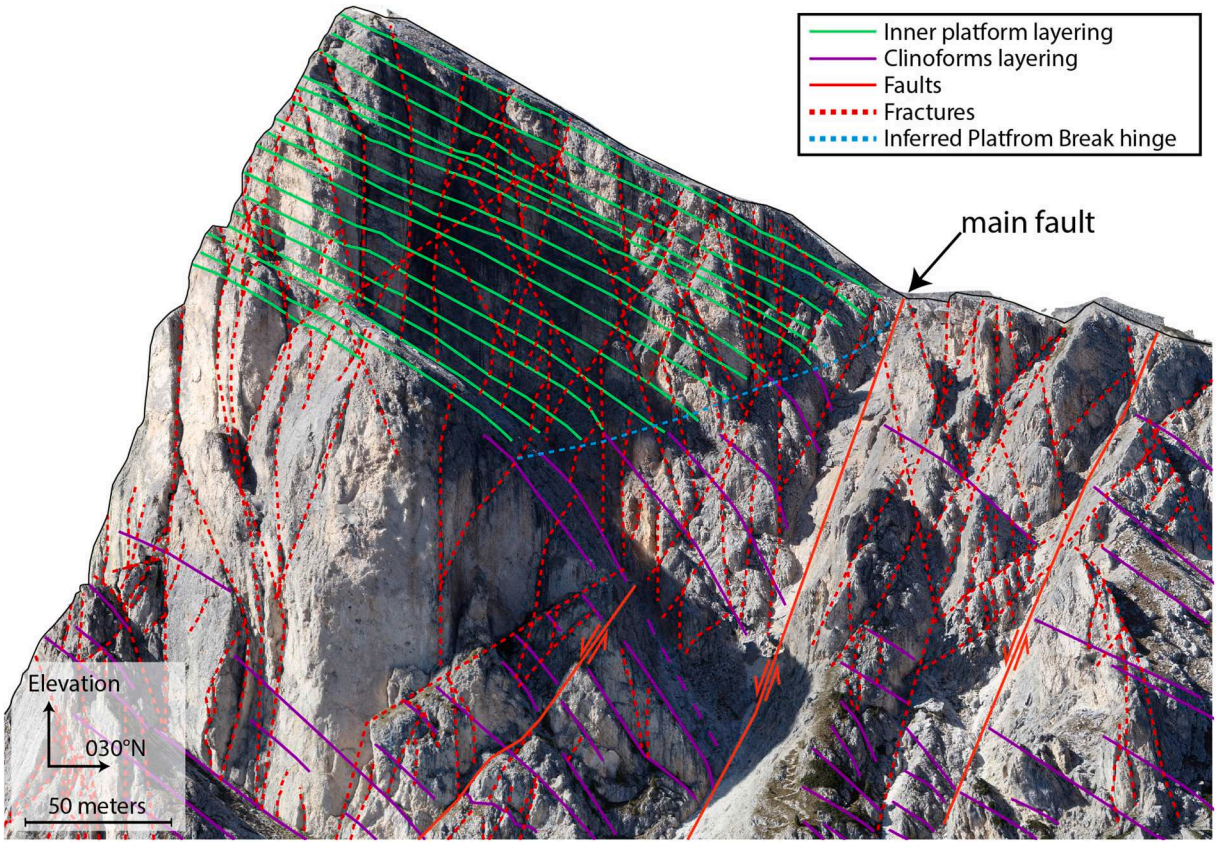

Fig. 9. Interpreted orthographic view of the upper-southern portion of the East cliff of the Gusela del Nuvolau DOM. The inner platform strata increase their dip and thickness moving towards the Platform break hinge. Moreover, also the dip and thickness of the clinoforms (purple lines) increase moving closer to the fault, suggesting the presence of a rollover fold structure. (For interpretation of the references to colour in this figure legend, the reader is referred to the Web version of this article.)

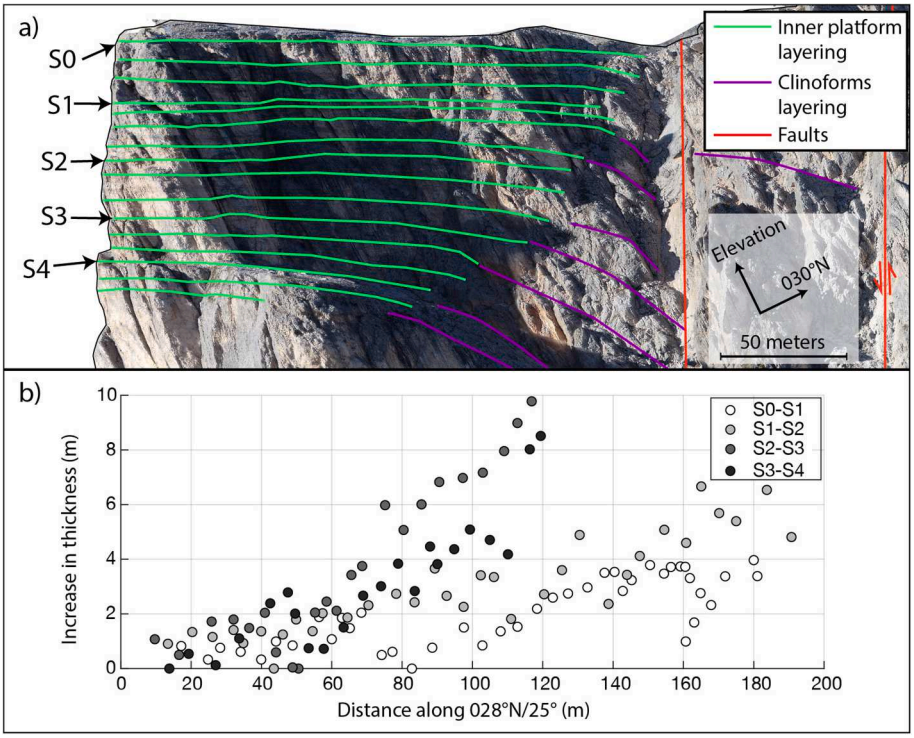

Fig. 10. (a) Orthographic and rotated view of the DOM area where the calculation of the thickness variation was performed. S0, S1, S2, S3 and S4 are the surfaces delimiting the packs of strata considered during the calculation. (b) Plot of the thickness variation (in meters) along the dip direction of the strata (028°N/25°), the thickness increase is calculated with respect to the thickness measured in the southern limit of the slope (close to black arrow). The measurements were performed using the tool 'Measure two-point thickness' of the Compass plugin of CloudCompare (Thiele et al., 2017), selecting the mean plane attitude of the inner platform beds and measuring the real thickness of the packs of strata along the normal vector of the mean plane.

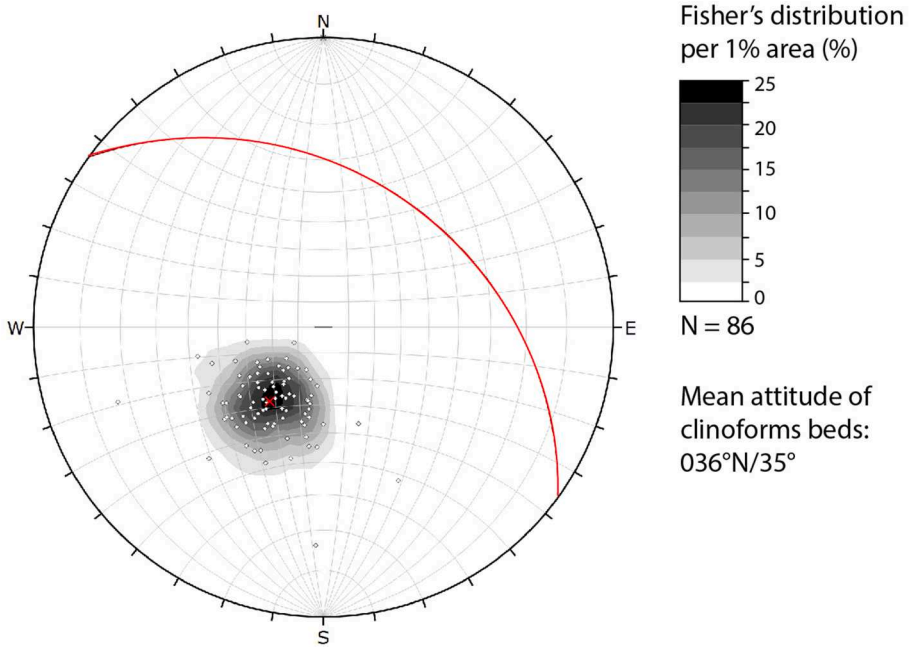

Fig. 11. Contour (lower hemisphere and equal angle projection) of the poles of the clinoforms. A progressive increase of the inclination is registered towards the basin.

- K2, with a sub-vertical and N-trending attitude;
- K3, the less abundant set with a sub-vertical and NE-trending attitude.

These orientations show a good coherence with those evaluated by the 2D fracture analysis, suggesting the presence of two main sets NW and ~N trending. The slight difference in the K2 trend observed in the two analyses is probably due to the bias of the 2D analysis because the fracture traces are mapped onto a N-dipping surface (top of the outcrop) causing an incorrect estimation of the fracture trends. The recognition of K3 set only in the 3D analysis is probably due to the easier exposure of these fractures onto the rock cliff.

Four main faults that affect the carbonate platform have been detected along the east cliff of the outcrop. They have the same direction of the K1 set, however they have a lesser inclination than the fractures belonging to this set, dipping toward ~220°N and displaying a curved shape (listric geometry), and an inclination that progressively decreases towards the base of the outcrop, passing from about 75° to 60° (average

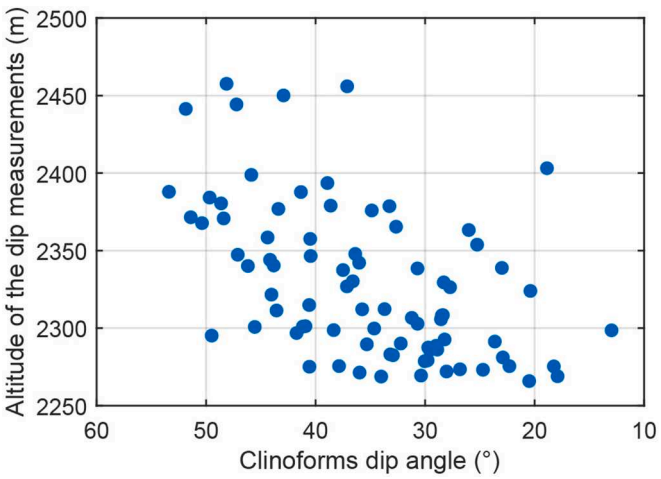

Fig. 12. Plot of the dip angles of the clinoforms versus the altitude at which the measures are performed. Although the data show a scattered pattern, they suggest a weak positive correlation.

inclination of all faults of 62°–71° - Fig. 21).

They dislocate the top of the basinal deposits that underlie the platform with a normal displacement of a few meters. No kinematic indicators were detected along these listric faults nor in the accessible part of platform nor in the basinal deposits, however the ductile deformations visible in these last sediments seem to confirm their normal displacement (see Figs. 16 and 17). Moreover, along the footwall of the two central and more extended faults, roll-over anticlines associated with an appreciable thickening of the clinoform beds can be observed (Fig. 22). This interpretation is based on the visible progressively and continuous increasing of the curvature of the bed surfaces towards the fault, on their abrupt interruption on the structure, as well as on the progressive thickening towards the faults of some clinoforms.

These structures and in particular the variation in thickness of the strata, indicate a probable synsedimentary activity. The ductile deformations locally affecting the basinal deposits below the normal faults and the clinoforms are in agreement with the fault displacement and can be explained by differential compaction under the weight of carbonate clastic deposits prograding from the inner platform towards the basin.

After the rotation of the DOM the faults and main fractures belonging to sets K2 and K3 assume a nearly vertical geometry; only the K1 set (minor fractures) appears to be less steep, with a mean dip of 65°. (Fig. 23).

6. Discussion

The Gusela del Nuvolau was already cited in the literature as a spectacular outcrop of Cassian carbonate platform where the relations between inner platform, slope and basin are well exposed (Bosellini, 1984; Blendinger and Blendinger, 1989). Notwithstanding, until recent years most of the observations were only possible from improper or distant points of view (e.g. from the base of the rock cliff or the top of the distant, 1–2 km, Lastoni di Formin massif) that can affect negatively the overall interpretation, introducing many biases. Thanks to the UAV-based digital photogrammetry, it has been possible to develop an accurate high-resolution DOM of the Gusela del Nuvolau outcrop (Figs. 4 and 5) whose analysis can overcome the main limitation of the traditional studies (Menegoni et al., 2018) and allow to obtain reliable measurements and interpretations (Inama et al., 2020).

Three different facies of the platform can be observed on the DOM (Fig. 7):

- inner platform facies, composed by well stratified, regular and plane parallel layers with a mean thickness of ~2 m;
- slope facies, characterized by thick and massive clinoform strata with a less marked layering;
- basinal facies, characterized by strongly marked, plane parallel and regular layers with a mean spacing of ~20 cm.

Moreover, the DOM structural analysis has allowed to identify four main normal faults and different sets of fractures affecting the outcrop and which are characterized by a high inclination (Figs. 20 and 21):

- K1 set, composed by faults and fractures dipping toward ~220°N.

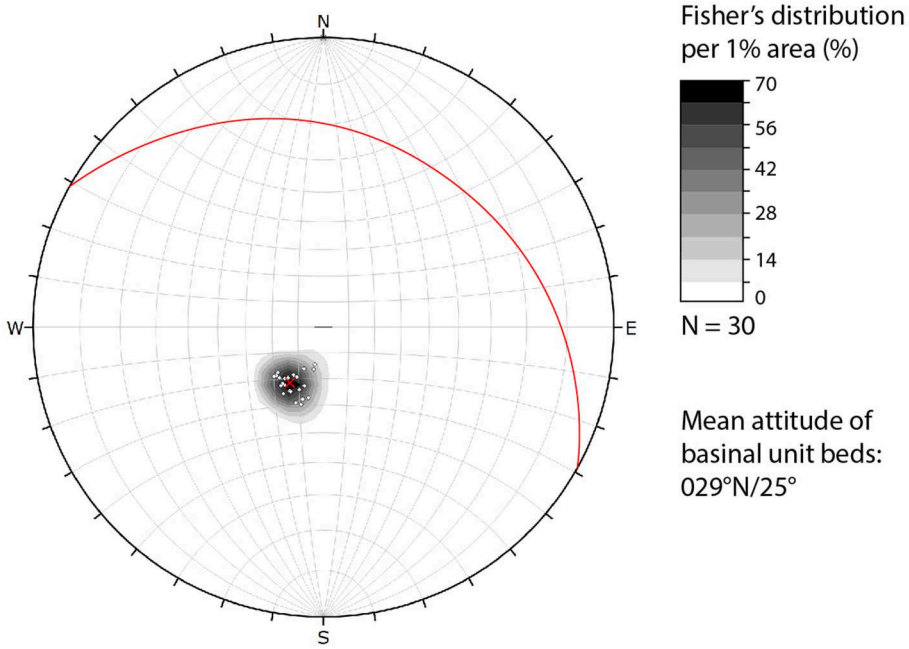

Fig. 13. Contour and lower hemisphere and equal angle projection of the poles of the basinal unit beds attitude. The red lines and cross mark the mean plane and pole, respectively. Only the regular and tabular beds attitudes are projected. (For interpretation of the references to colour in this figure legend, the reader is referred to the Web version of this article.)

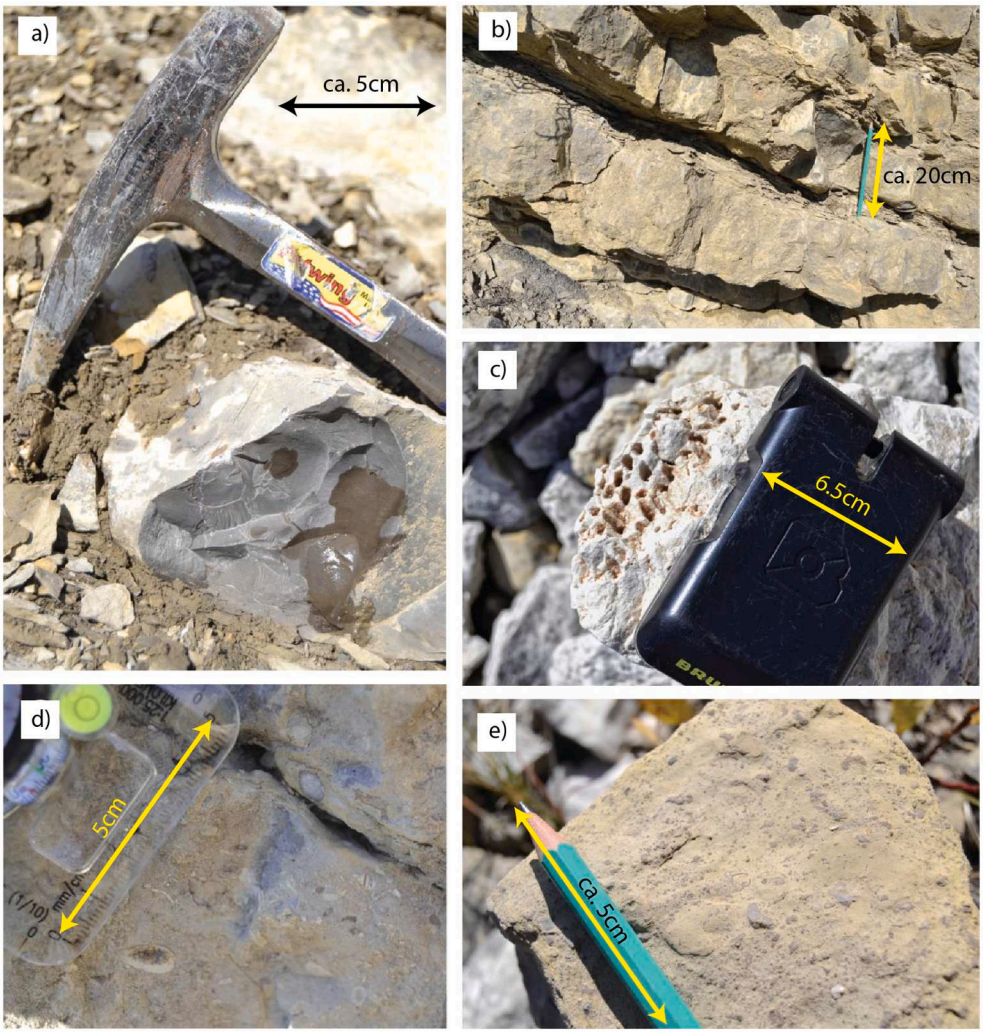

Fig. 14. Details of the San Cassiano Fm. (basinal facies) visible in the lower part of the rock cliff where access is possible. (a) Grayish fresh surface of the carbonatic component. (b) Regular layering of basinal deposits with the alternation of erodible beds and more competent strata. (c) Dolomitized coral patch-reef. (d), (e) Bioclastic and intraclastic components of the San Cassian Fm (after Passoni, 2020).

- K2, composed by faults and fractures dipping toward ~260°N.
- K3, composed by faults and fractures dipping toward ~310°N.

The relative orientations of these sets seem to be pretty similar to those detected in the study of Inama et al. (2020) onto the nearby Lastoni di Formin outcrop, with a probable overall clockwise-rotation of about 10° toward East.

6.1. Direction of progradation

The actual geometries and attitudes of the exposed platform suggest a NE direction of progradation onto the San Cassiano basinal unit, which is confirmed also after the platform restoration realized bringing the inner platform beds back to the horizontal (Fig. 18). This direction of progradation agrees with that described by previous interpretations, where the Gusela del Nuvolau is depicted as a NE step-wise prograding platform (Bosellini, 1984) with a restored clinoforms dip of around 5° (Blendinger and Blendinger, 1989).

6.2. Clinoforms geometry

Investigating accurately the 3D orientation of the clinoforms, it has been possible to determine that they dip toward NE (actual dip direction 036°N, restored one 055°N) with angles higher than the 5°, proposed by Blendinger and Blendinger (1989). The restored dip angles are very variable (Fig. 24), but show a maximum frequency around 12°–15°.

The 3D analysis of the DOM suggests an oblique-tangent shape of the clinoforms: steeper in its central part and less steep at its toes. This suggestion seems also confirmed by the clinoforms dip angle measurements (Fig. 12) that show a weak positive correlation with the altitudes at which the measurements are performed: at higher altitudes higher dip angles are measured while at lower quotes (towards the basin) dip angles decrease.

Notwithstanding, the presence of faults that cut the entire outcrop and the consequent impossibility to follow the entire clinoforms from the platform-break hinge to the downlap surface hampers an accurate analysis of the dip change along clinoforms.

6.3. Slope-to-basin transition geometry

The previous study of Bosellini (1984) identifies the Gusela dal Nuvolau outcrop as an excellent example of step-wise progradation toward N-NE of the Cassian platform-margin talus slope over bedded basinal San Cassian sediments. Bosellini (1984) describes this geometry as the results of "episodic processes of massive debris input, during which the platform margin advances, alternated with long periods of non-sedimentation during which basinal sediments accrete and onlap the platform" slope, creating an interfingering geometry.

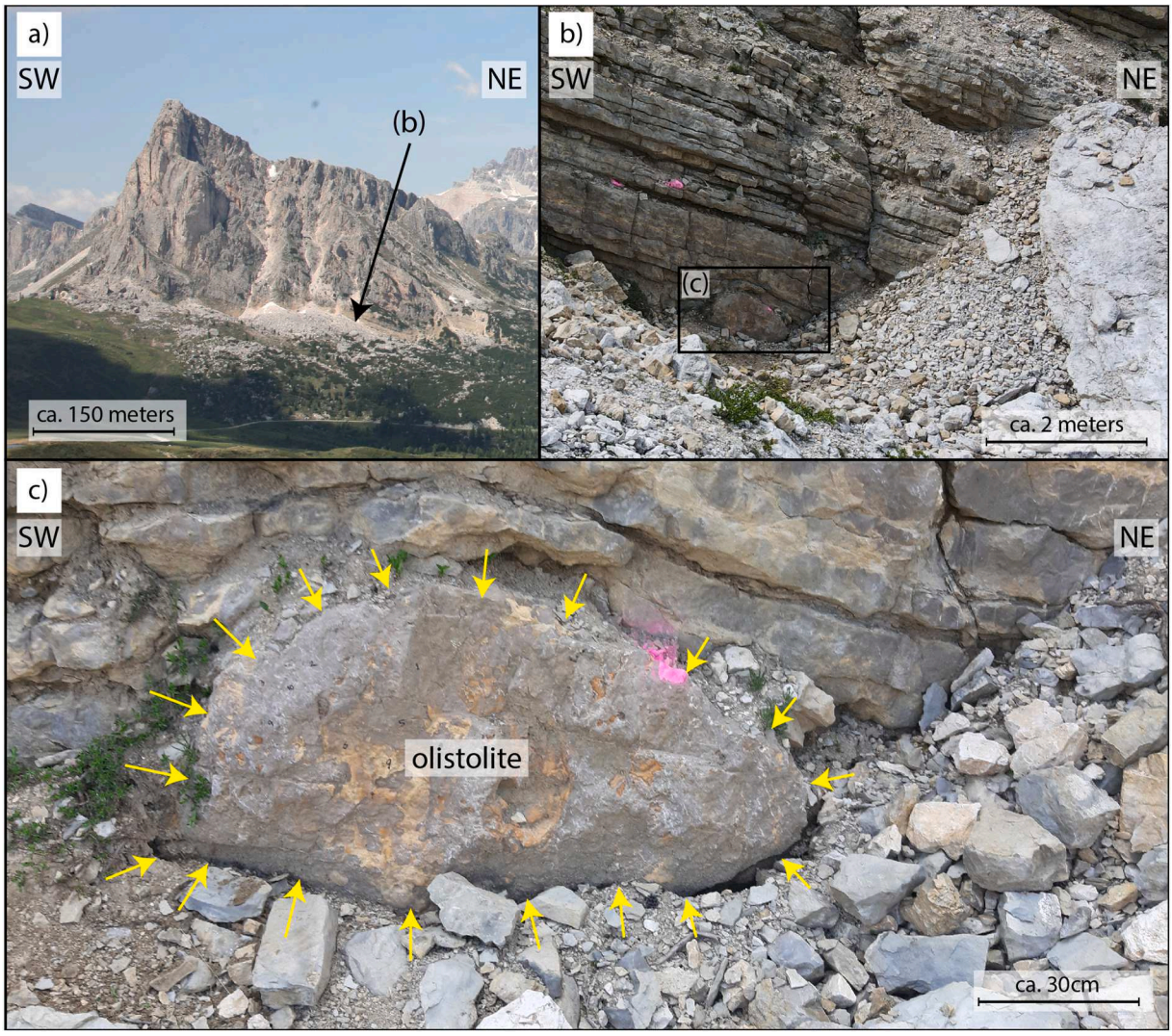

Fig. 15. (a) Photographs of the Gusela del Nuvolau east cliff, where in the lower part of slope outcrops the basinal facies represented by the San Cassiano Formation (b) and some metric olistolites are visible (c).

During the 3D model analysis, the step-wise geometry of the slope-basin contact proposed by Bosellini (1984) was effectively verified, while no clear interfingering or onlap phenomena were detected. The irregular slope-basin boundary seems essentially due to the presence of faults dipping towards the inner platform and ductile deformations affecting the San Cassiano beds, both probably related to differential compaction of the basinal sediments (Figs. 16 and 17).

6.4. *Early deformations due to differential compaction*

Different studies (Saller, 1996; Hunt and Fitchen, 1999; Rusciedelli and Di Simone, 2007; Berra and Carminati, 2012; Resor and Flodin, 2010; Berra et al., 2016) show as the differential compaction processes could cause different syndepositional or syndiagenetic deformations in carbonate platforms, from stratal architecture modification to syndepositional/syndiagenetic fracturing and folding. In general, differential compaction happens when the thickness of the compactable unit or the compactional load is not uniform. During the analysis of the Gusela del Nuvolau DOM, numerous evidences of differential compaction-driven early deformations were found.

The first evidence concerns the inner platform stratal architecture. The 3D model allows us to estimate that the inner platform strata thickness and dips increase toward the margin of the platform (Fig. 11). This behavior was already documented by Inama et al. (2020) and Doglioni and Goldhammer (1988) for the nearby and coeval Cassian platforms of the Lastoni di Formin and Sella, respectively. This mechanisms could be related to the non-uniform compaction of the basinal unit caused by the differential thickness of the basinal unit (e.g. Doglioni and Goldhammer, 1988; Berra and Carminati, 2012; Berra et al., 2016) and/or the differential load caused by the irregular geometry of clinoforms (Hunt & Fitchen, 1999). In both cases, the inner platform beds are bended-down toward the basin with an increase of their thickness and dips for the differential compaction of the basin unit, but whereas in the first cases this is due to the geometry of the basinal unit, the latter is due to the geometry of the carbonate platform (Fig. 25).

This scenario is also confirmed by the folds affecting the basinal deposits of the San Cassiano Formation that have been detected at the base of the platform. They are visible under the irregular steps that characterize the lower boundary of the buildup, indicate a major differential lowering of the basin towards the inner platform, and are characterized by a sub-horizontal axis whose trend is orthogonal to the direction of progradation.

Another possible evidence is related particularly to one of the main faults that cut the entire outcrop. The fault is a high angle listric normal fault that dips towards SW, belongs to the K1 set and moves down the SW block (hanging wall). The clinoforms of the hanging wall near the

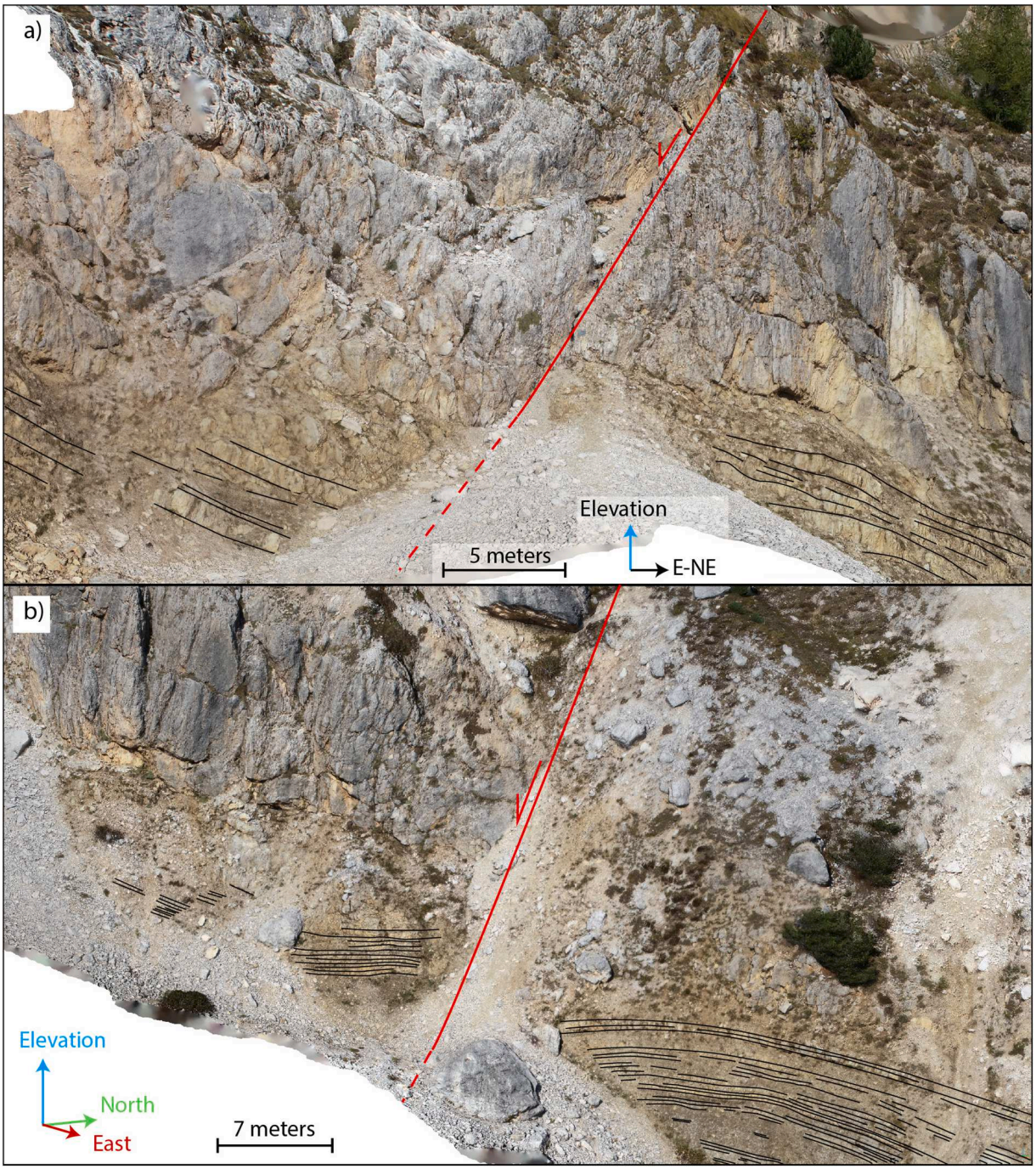

Fig. 16. (a) (b) High resolution orthographic views of the Gusela del Nuvolau DOM, where the deformations at the slope-basin contact are visible. The normal faults, marked in red, dip toward SW about 70°. In (b) the displacement is partially masked by talus. (For interpretation of the references to colour in this figure legend, the reader is referred to the Web version of this article.)

fault surface are affected by a probable rollover anticline and show an increase of thickness towards the fault suggesting its possible syn-depositional deformation (Fig. 22).

However, the intense fracturing affecting the margin of the carbonate platform partially masks the structure.

From the analysis of DOM of the Gusela Del Nuvolau, it cannot be excluded that some of these deformations (Figs. 10 and 22) may be ascribed to depositional geometries of the carbonate platform. It has been demonstrated that some Early Carnian carbonate platforms of the Dolomites were microbial platforms (Preto et al., 2017 and reference within). Some research on microbial platforms (Sierra della Cuenta in Della Porta et al., 2004 and Kenter et al., 2005; Latemar in Marangon et al., 2011; Latemar and Sella in Preto et al., 2017) show as they tend to develop margins that deepens towards the slopes (basinward-dipping strata, also called 'fall-in strata'), with the outermost facies of the inner platform subtidal and less well stratified. However, in microbial platforms, the possible seaward bed thickening develops at the base and not in the upper part of the slope as in the case of Nuvolau.

Moreover, due the pervasive dolomitization of the platform that often completely obliterates the original texture of the rocks, it was not possible to assess the real microbial nature of the Nuvolau platform and, therefore, to discriminate the deformations due to differential compaction from the original depositional geometries.

To better understand the possible consequences on the carbonate

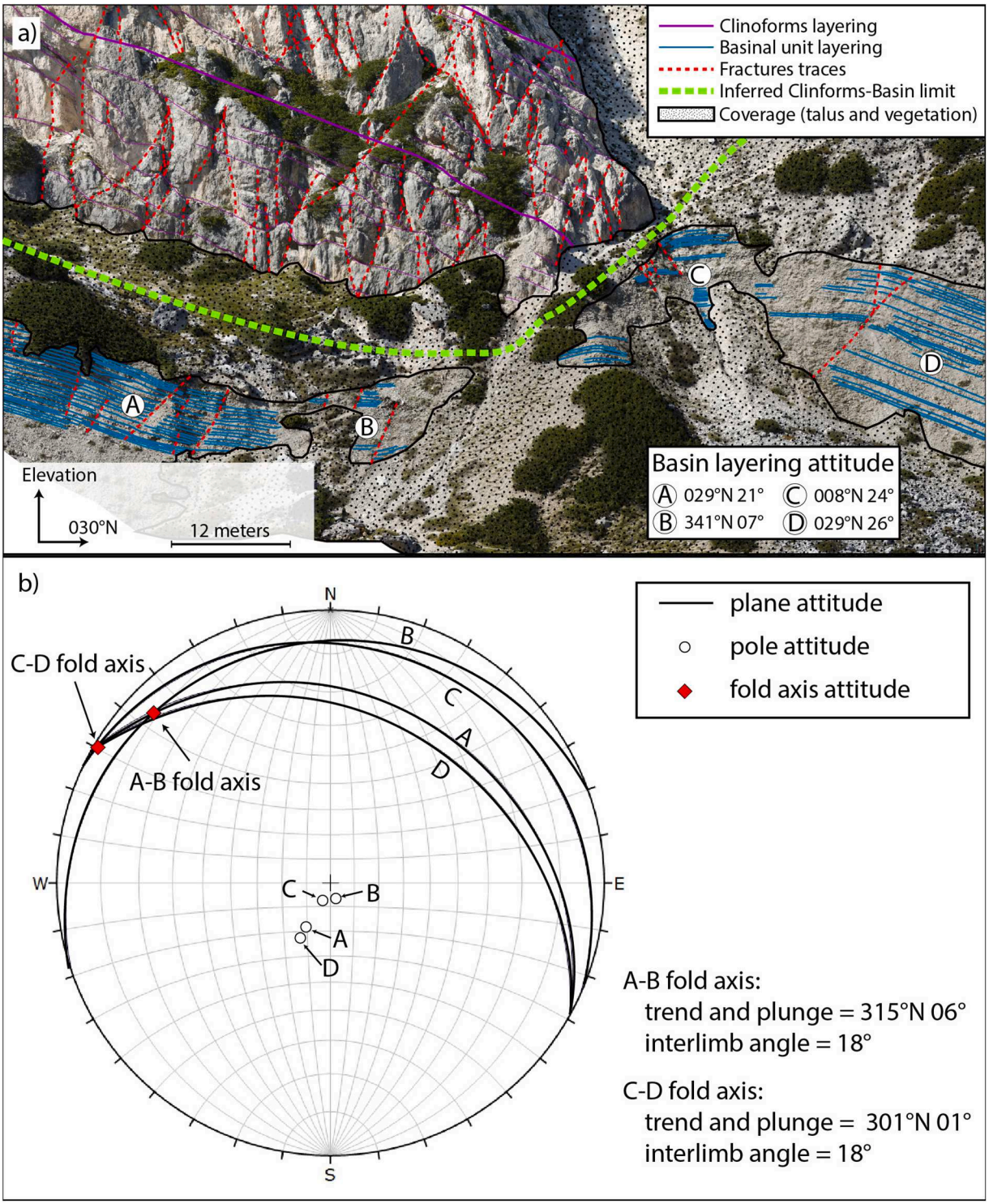

Fig. 17. (a) Interpreted detail of the DOM near the termination of the clinoforms and the slope to basin transition. The San Cassiano formation is folded in correspondence of the clinoforms terminations, with a sub-horizontal fold axis trending around 301°-315°N.

platform of the differential compaction of the underlying basin unit, we performed a 2D compaction model using the *2D Decompaction* module of the software MOVE (Petroleum Experts). This module can be used to decompact or compact a succession according to the traditional *porosity-depth change* method (Athy, 1930; Rubey and Hubert, 1959; Sclater and Christie, 1980; Schmoker and Halley, 1982). Among the several empirical curves presented in the literature that describe the relationship between porosity and depth, we used the single term exponential curves proposed by Sclater and Christie (1980). Whereas the basinal unit was considered compactable, the carbonate platform was considered virtually uncompactable. The parameters of the basinal unit used for the compaction model correspond to chalk parameters, defined by Sclater and Christie (1980), and are indicated in Table 3.

We decided to use the chalk parameters to emphasize the differential compaction effects.

Doglioni and Goldhammer (1988) already depict the possible contribution of the differential thickness of the basinal unit onto the differential compaction process onto the coeval Cassian platform of

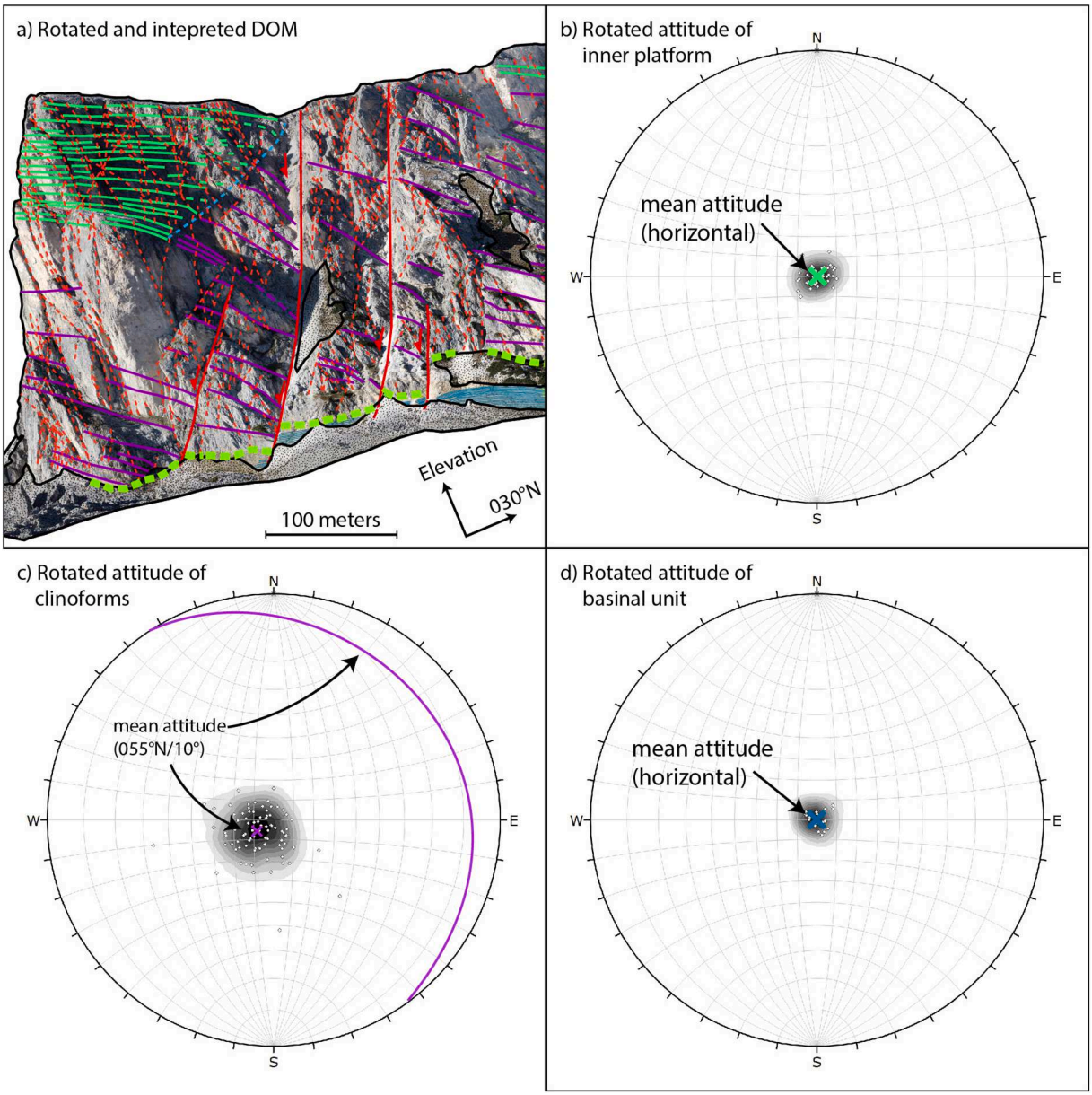

Fig. 18. (a) Interpreted DOM of the Gusela del Nuvolau after the restoration (for the legend see Fig. 8b). Stereoplots of the restored attitude of (b) inner platform beds, (c) clinoforms and (d) basinal unit. The restoration consists of a clockwise rotation of 25° around an axis 118°N/0° (trend and plunge). The rotation allows restoring at their possible initial horizontal configuration the inner platform and basinal strata.

Sella, but do not consider the possible effect due to the platform geometry.

According to Hunt and Fitchen (1999), the compactional load is mainly influenced by the mechanism and geometry of progradation and aggradation acting at the margin of a carbonate platform. Therefore, we developed an initial compaction model (t = 0) with a 300 m thick, flat and compactable basinal unit overlaid by a 50 m thick uncompactable carbonate platform with a straight slope inclined of 30° (Fig. 26).

The initial geometry of the compaction model was set-up considering the thickness of the basinal unit, the San Cassiano formation, measurable onto the Italian geological cartography at scale 1:50,000 of the study area - the *Foglio - 29 Cortina d'Ampezzo* of the CARG project described by Neri et al. (2007) and retrievable online at ISPRA catalogue (https://www.isprambiente.gov.it/Media/carg/29_CORTINA_-DAMPEZZO/Foglio.html) - and a low carbonate platform height, in order to simulate a successive growth phase. Moreover, it has been decided to locate the slope to basin transition far from the model boundary in order to avoid numerical artifacts. It is important to emphasize that this model set-up does not want to represent the exact geometry and/or evolution of the Gusela del Nuvolau, but simply to describe the possible deformations caused by differential compaction.

The deformed geometry (t = 1) achieved after the first compaction was then used to develop three different models of the platform growth with three different Progradation to Aggradation (PA) ratios: PA ratio equals to 0 corresponds to 0 m progradation and 50 m aggradation; PA ratio equals to 1 corresponds to 50 m progradation and 50 m aggradation; PA ratio equals to 10 corresponds to 50 m progradation and 5 m aggradation. This second stage of compaction (t = 2) was performed considering only the new developed carbonate platform as the compactional load (Fig. 27).

The results of all the models (Figs. 26b and 27) show that the maximum compaction of the basinal unit due to the load of the carbonate platform is always located below the inner platform, where the carbonate body has the greater thickness, and that the downslope plane

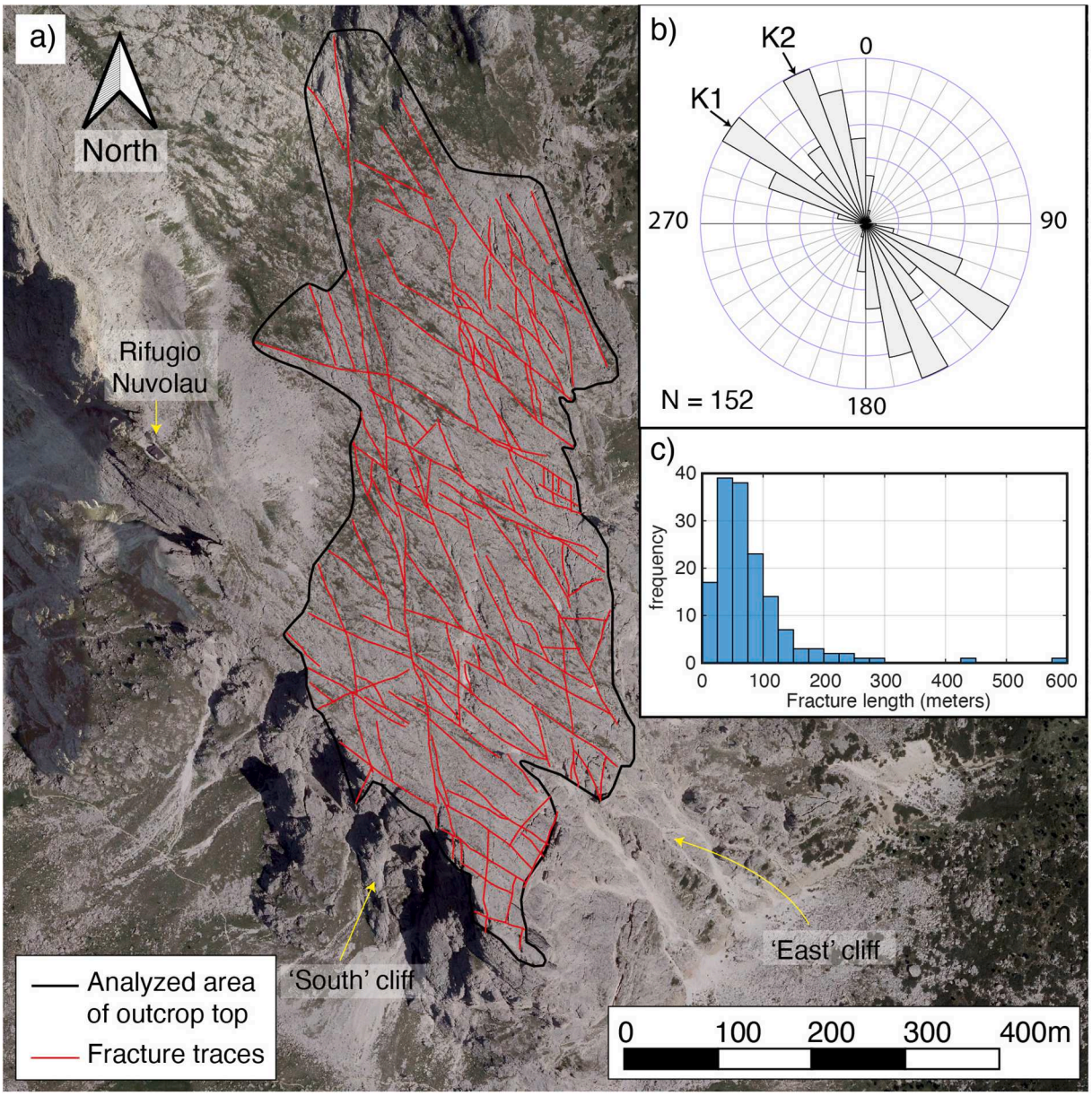

Fig. 19. (a) Orthoimages of top of the Gusela del Nuvolau outcrop and fracture traces mapped during the 2D analysis. (b) Rose plot of the fracture traces azimuth suggesting the presence of two main fractures sets (bins dimension is 10°). (c) Histogram of the fracture trace length (bins dimension is 25 m) displays a log-normal distribution.

always modifies its attitude, dipping toward the platform.

The models that underwent a second stage of compaction due to further growth of the carbonate platform show that differential compaction causes climbing progradation-like platform geometry and a deformation of the slope (Fig. 27) that assumes a shape from straight to concave-up, with dip angles that progressively decrease from the upper slope to the toe of the slope.

Moreover, the compaction models with PA ratios equal to 1 and 10 (prograding platform) display a tilting of the platform margin toward the basin also in this case caused by the differential compaction of the underlying basinal unit. It cannot be excluded that this phenomenon may favor the progressive curvature of the normal faults which can affect the margin and the slope of the platform.

In general, the results of the compaction models fit well with the deformations visible at the Gusela del Nuvolau, strengthening the hypothesis that these could be differential compaction-driven early deformations. In particular, the transition zone connecting the platform margin with the basin, which includes the whole area of the slope, is subjected to the most relevant differential subsidence due to differential compaction of the underlying basinal sediments. It is therefore reasonable to assume that this is the sector most subject to fracturing and faulting and that the normal faults that can form tend to lower the blocks towards the inside of the carbonate platform.

6.5. *Fracture network*

The fracture network affecting the Gusela del Nuvolau is similar to that observed by Inama et al. (2020) onto the nearby Lastoni di Formin outcrop. Three main near-vertical fracture sets named K1, K2 and K3 and trending around 130°N, 170°N, and 40°N, respectively, have been detected. The only difference consists in the fact that the Gusela del Nuvolau fracture network is probably rotated about 10° toward East respect to the Lastoni di Formin one and that the K1 fracture set at the Gusela del Nuvolau cannot be discriminated in two subsets as in the

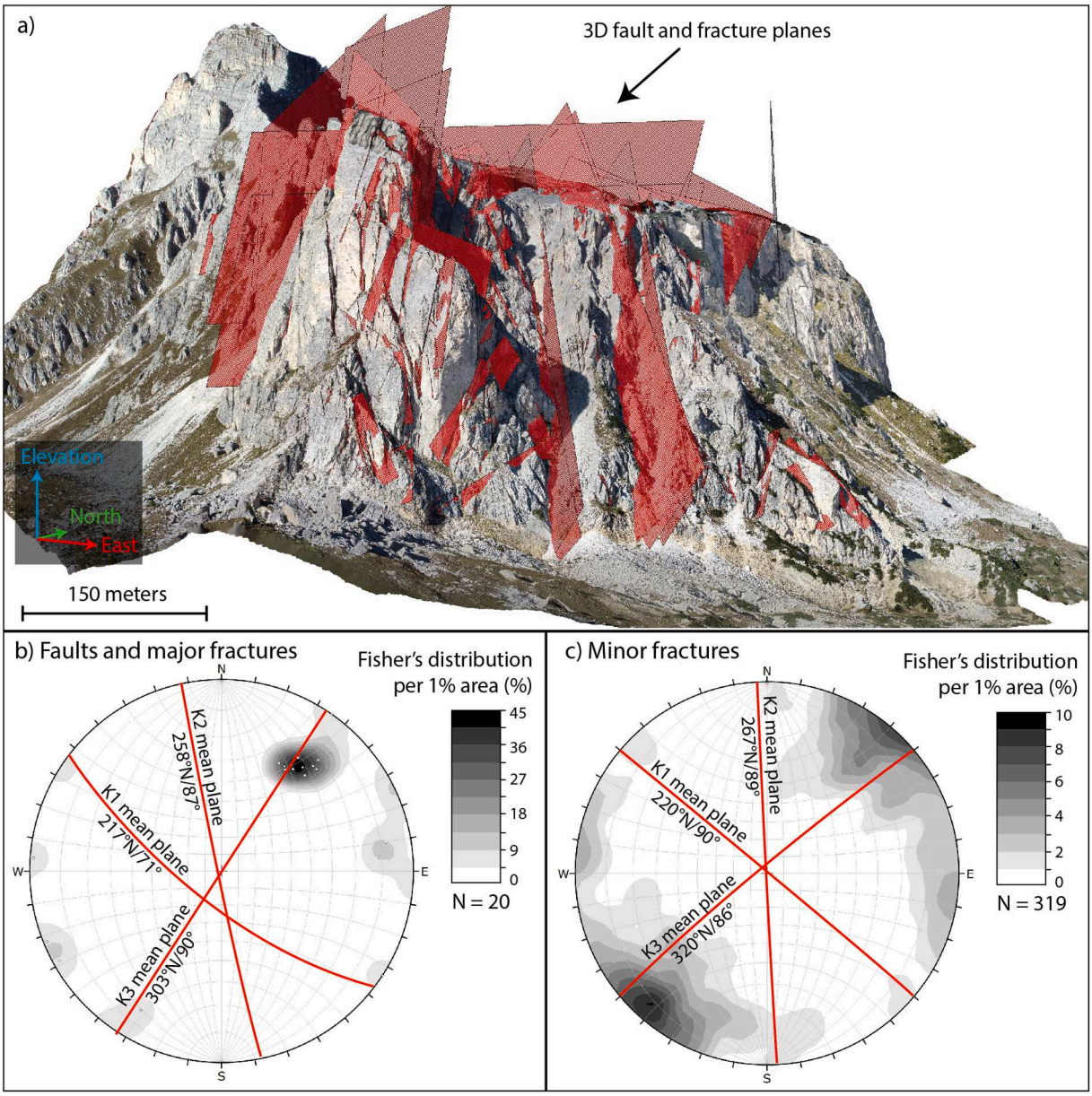

Fig. 20. (a) Oblique view of the Gusela del Nuvolau DOM with some principal 3D faults and fractures detected (marked by the red rectangles). (b) Contour of the poles of the recognized faults and major fractures and cyclographic projection of the mean planes of the different sets (lower hemisphere and equal angle projection). (c) Contour of the poles of the recognized minor fractures and cyclographic projection of the mean planes of the different sets (lower hemisphere and equal angle projection). Major and minor fractures are discriminated according to their size (higher or lower than 100 m, respectively). (For interpretation of the references to colour in this figure legend, the reader is referred to the Web version of this article.)

Lastoni di Formin outcrop (Inama et al., 2020; Inama, 2021). This last difference is probably due to the smaller dimensions of the Gusela del Nuvolau outcrop, where a large exposition of the top of the platform is missing.

The DOM-based fracture dataset show similarity with the fracture pattern recognized in some other Middle Triassic carbonate platforms of the Dolomites (e.g. Mollema and Antonellini, 1999; Boro et al., 2013; Hardebol et al., 2015). In particular, the accurate analysis performed by Mollema and Antonellini (1999) at the Sella complex, where part of a coeval Cassian platforms is exposed, show faults and fractures pattern similar to those obtained from our analysis (Fig. 20) describing the presence of three sets of strike-slip faults formed during Alpine orogeny for the localization and coalescence of opening-mode fractures However, in our opinion and according to Inama et al. (2020) interpretations, we believe that some of these faults and in particular the NW-SE striking structures are syndepositional normal faults caused by an early gravitational deformation of the platform possibly caused by the platform progradation and differential compaction-induced subsidence of the San Cassiano basinal deposits. These synsedimentary structures are oriented nearly perpendicular to the direction of progradation of the carbonate platform.

In fact, after the restoration of the original geometry of the Gusela del Nuvolau platform that was obtained by bringing the inner platform strata back to the horizontal K1 fracture set (Fig. 23) assume an attitude near-orthogonal to the direction of progradation (NE, around 55°N). the K1 major fractures generally become sub-vertical (mean dip of 85°, Fig. 23b), K1 normal faults dip towards SW, whereas the restored K1 minor fractures have a smaller angle of inclination (about 65°) with a near Andersonian attitude (Fig. 23c). These kinds of extensional fractures were already identified and deeply investigated by Inama et al.

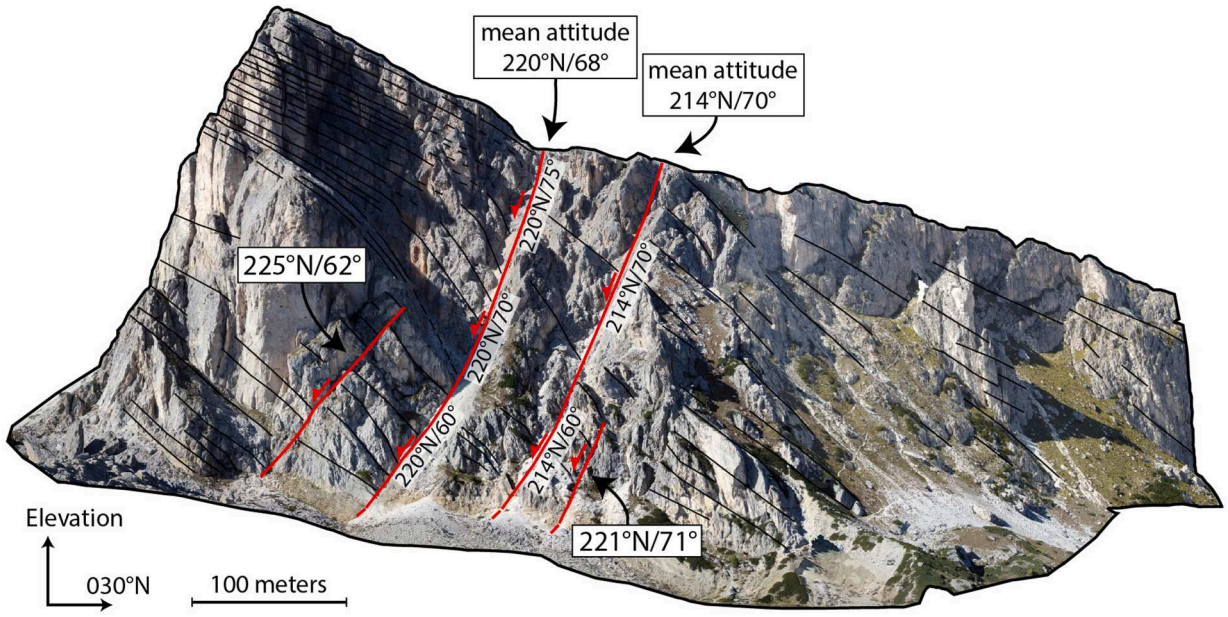

Fig. 21. Simplified interpretation of the orthographic view of the east cliff of the Gusela del Nuvolau, where the mean attitude of the main normal faults that affect the carbonate platform is shown. All the faults dip toward 214°-221°N with an mean angle of 62°–71°. These faults belong to the K1 set. For the two main faults in the central sector of the outcrop, the dip variation is shown.

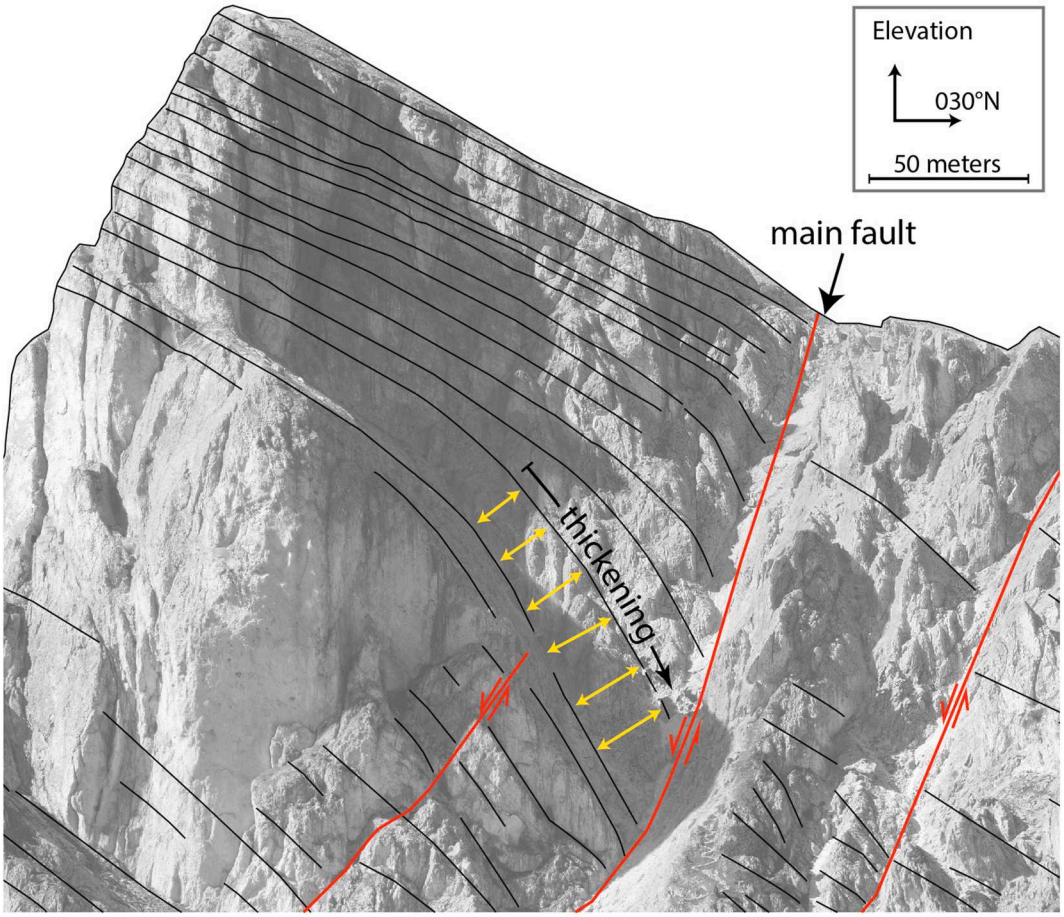

Fig. 22. Simplified interpretation of the Gusela del Nuvolau outcrop (black and red lines are strata and faults, respectively) where the increase of dip angle and thickness of the clinoforms suggest a possible rollover anticline. (For interpretation of the references to colour in this figure legend, the reader is referred to the Web version of this article.)

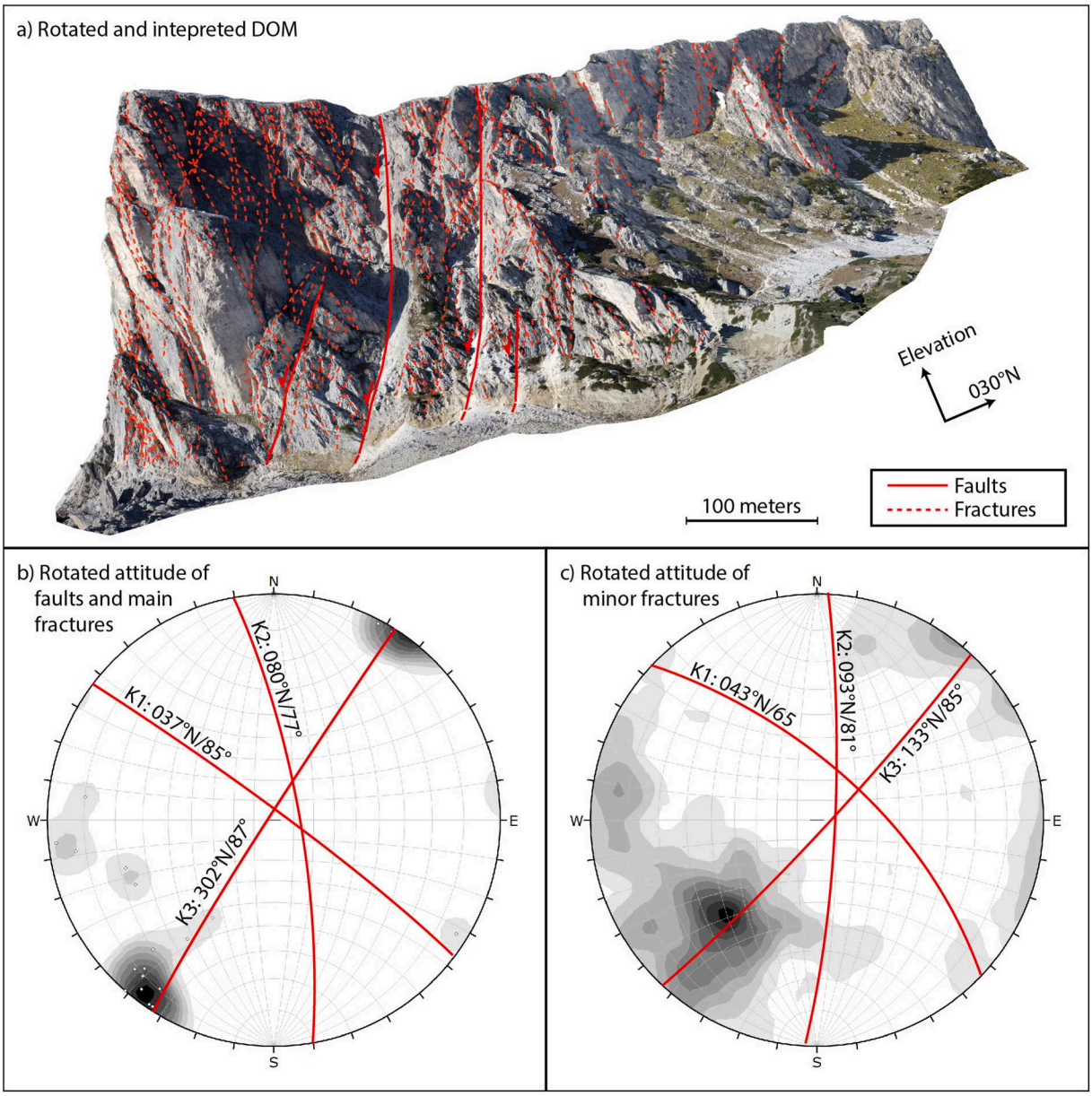

Fig. 23. (a) Rotated outcrop with its fracture network. (a) Stereoplots of rotated faults and major fractures and (b) minor fractures datasets. The contours of the stereoplots depict the density of the rotated fractures orientations, whereas the red lines depict the rotated mean plane of the fractures sets. (For interpretation of the references to colour in this figure legend, the reader is referred to the Web version of this article.)

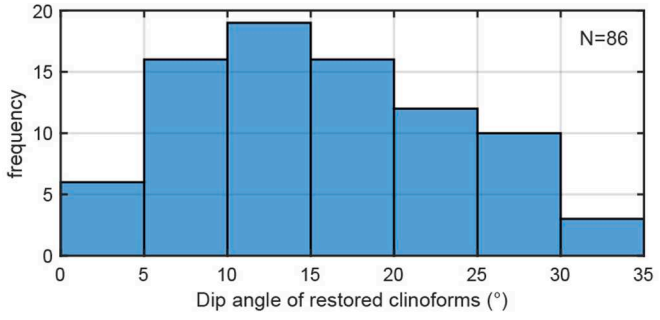

Fig. 24. Histogram of the dip angle of the restored clinoforms showing a high variability of the dip values. The maximum frequency is around 12°–15°.

(2020) onto the Lastoni di Formin outcrop interpreting them as syndepositional fractures. Comparison of field data orientation on the Lastoni di Formin confirms the probable early age of many K1 structures showing that this set, widely present on the platform top, is much less present in the overlying Heiligkreuz Fm, deposited after the demise of the Lastoni buildup. Moreover, Inama (2021) after a kinematic and cross-cutting relationship analysis of the fault and fracture network affecting the closer and coeval Cassian carbonate platform of the Lastoni di Formin show that the outcropping K1 normal faults (with metric offsets toward the platform interior) are related to the synsedimentary deformation and predated the Jurassic K2 set and a set of vertical a dextral strike-slip faults with a W-E trend.

However, it should be clearly emphasized that not all K1 fractures are synsedimentary and that all the fractures show signs of successive reactivations. Moreover, the exact quantification of the incidence of syndepositional fracturation, as well as any correlation with the main facies of the platform, is strongly inhibited by the current condition of

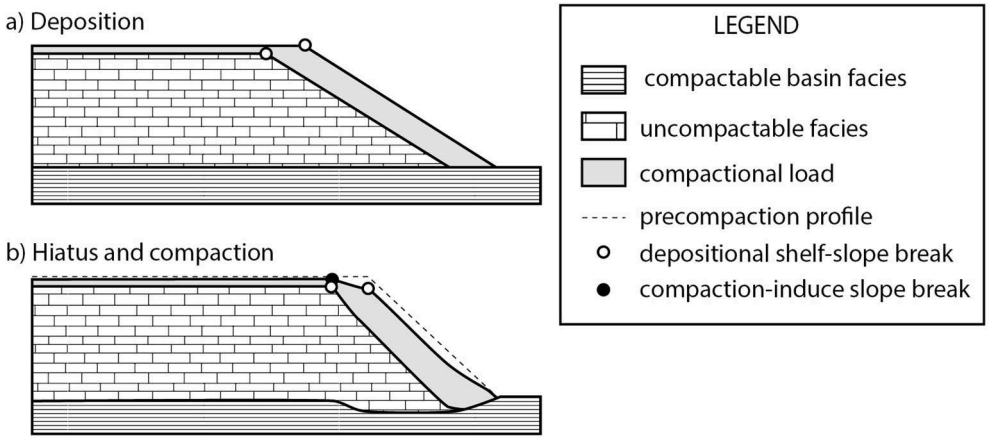

Fig. 25. Sketch model of the differential compaction caused by differential compactional load (redrawn after Hunt and Fitchen, 1999). (a) Geometry of the carbonate platform (uncompactable facies) and basin (compactable facies) after an episode of deposition of carbonate platform facies (compactional load) and (b) geometry after the depositional hiatus and compactional. The different geometry of the compactional load (mostly due to clinoforms) causes differential compaction of the basin facies and, therefore, syn-depositional deformation of the uncompactable carbonate platform facies.

Table 3
Parameters used to perform the 2D compaction model.

Stratigraphic unit	Density	Initial porosity	Depth coefficient
Carbonate platform	2700 kg/m^3	N/D	N/D
Basin	2200 kg/m^3	0.70	0.71 km^{-1}

the outcrop, pervasively dolomitized and affected by several deformational events occurred over times.

7. Conclusions

The field survey of the carbonate platform of the Gusela the Nuvolau was integrated using the UAV-based digital photogrammetry, with the interpretation of high accuracy and resolution Digital Outcrop Model (DOM). This technique permits overcoming the main limitation of the

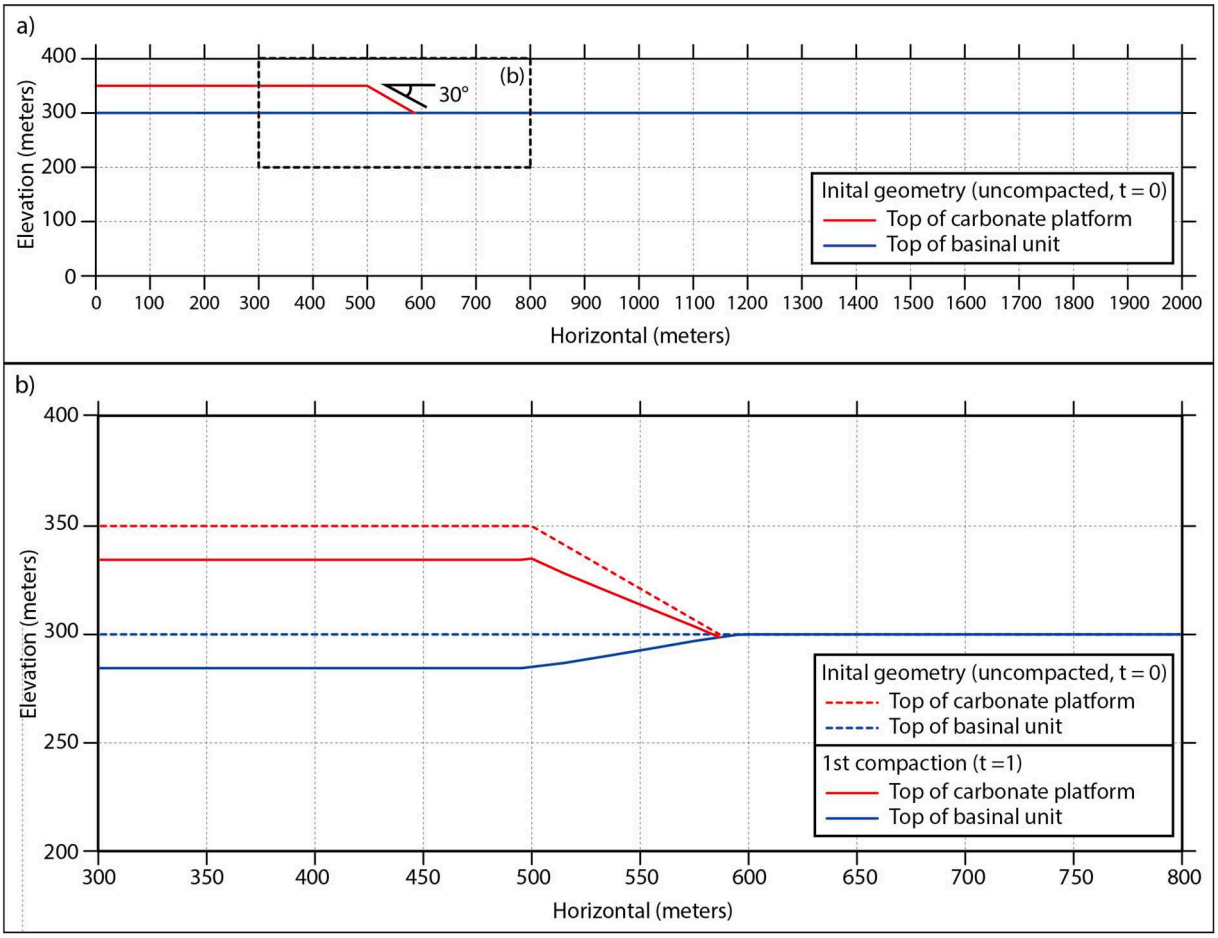

Fig. 26. (a) Initial geometry (t = 0) of the model. (b) Detailed view of the model after the compaction performed using the Decompaction tool of the MOVE software (Petroleum Experts). The compaction is constant in the inner part of the platform (at the left of the platform break), where the compactional load is constant, and decreases along the slope towards the basin where the compaction load decreases.

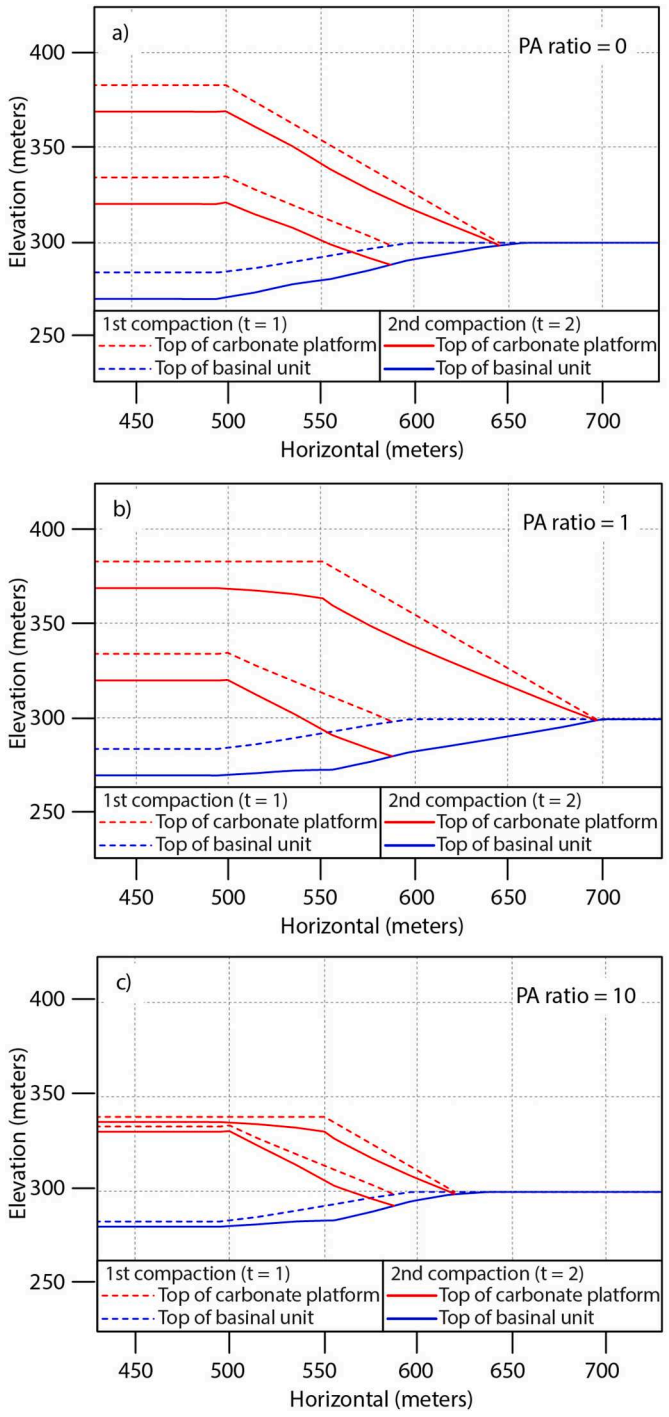

Fig. 27. Results of the second stage of compaction after the growth of a new part of the carbonate platform. (a)(b)(c) depict the compacted models with Progradation to Aggradation (PA) ratios equal to 0, 1 and 10, respectively. All models show after the compaction a concave-up shape of the slope. The models referring to the PA ratios equal to 1 and 10 show a tilting of the platform margin toward the basin.

traditional field survey, such as the impossibility to reach the inaccessible portion of the outcrop and the interpretation biases related to the non-optimal point of view.

The study allowed to define quantitatively the geometrical features of the Cassian carbonate platform and, in particular, of its platform-slope-basin transitional zone. Locally, after the restoration of the platform at its original attitude (realized by bringing the inner platform bedding back to the horizontal), the platform break and the downslope planes show an angle of about 36° and 15°, respectively, dipping toward SW, while the dip of the different generations of clinoforms have an angle encompassed between 5° (near the toe of the slope) and 35° (at the upper slope) and indicate a direction of progradation towards NE.

The study of this area highlighted also the presence of early deformations affecting the platform margin. In particular, a progressive increase of the thickness and dip of the inner platform bedding can be observed towards the margin and some early normal listric faults dipping with a high angle towards the inner platform with a trend orthogonal to the direction of progradation have been detected. In particular, one of these structures is associated with a roll-over anticline affecting the hanging wall clinoforms that also show a thickening towards the fault. These deformations have been interpreted as due to the differential compaction of the San Cassiano basinal Formation under the load of the platform margin that may have induced a greater lowering of the sectors towards the internal platform (the normal faults generally dip towards the inner platform). This detected early extensional fault suggests a possible early genesis of some other faults and fractures that belongs to the same K1 set that developed nearly parallel to the platform margin. Based on their morphological expression and their orientation, a correlation of these early faults and joints with the differential subsidence suffered by the buildup is strongly probable (see Inama et al., 2020).

The existence of gravitational-driven early deformations linked to differential compaction seems also confirmed by the folds affecting the basinal strata of the San Cassiano Formation that have been detected at the base of the platform. They have a sub-horizontal axis whose trend is orthogonal to the direction of progradation and have been observed under the irregular steps that characterize the lower boundary of the platform.

The outcomes numerical modeling of the differential compaction process are in good agreement with the DOM-based observations, and, allow to confirm the presence of early-deformation structures driven by gravitational processes.

However, the impossibility of an analysis of the microfacies due to the strong and pervasive dolomitization affecting the carbonate platform, does not allow to exclude that the geometries identified as effects of differential compaction process may be due to a possible microbial nature of the carbonate platform itself (see e.g. Cassian platform of Sella), which may have been partially modified by syndepositional and more recent faults and fractures.

Authors contributions

Niccolò Menegoni: Conceptualization, Methodology, Software, Validation, Formal analysis, Investigation, Resources, Data curation, Writing – original draft, Visualization, Writing – review & editing. **Riccardo Inama:** Conceptualization, Methodology, Software, Validation, Formal analysis, Investigation, Resources, Data curation, Writing – original draft, Visualization, Writing – review & editing. **Matteo Crozi:** Drone flights execution. **Cesare Perotti:** Conceptualization, Methodology, Software, Validation, Formal analysis, Investigation, Resources, Data curation, Writing – original draft, Visualization, Writing – review & editing, Supervision, Project administration.

Declaration of competing interest

The authors declare that they have no known competing financial interests or personal relationships that could have appeared to influence the work reported in this paper.

Acknowledgment

Petroleum Experts are acknowledged for the donation of MOVE academic licenses to the University of Pavia. We would also like to thank Nereo Preto and an anonymous Reviewer whose comments and

suggestions have helped us to improve and clarify this manuscript.

References

Adams, E.W., Schlager, W., 2000. Basic types of submarine slope curvature. J. Sediment. Res. 70, 814–828. https://doi.org/10.1306/2DC4093A-0E47-11D7-8643000102C1865D.

Antonellini, M., Mollema, P., 2000. A Natural Analog for a Fractured and Faulted Reservoir in Dolomite: Triassic Sella Group, Northern Italy. AAPG Bull. 84 (3), 314–344. https://doi.org/10.1306/C9EBCDDD-1735-11D7-8645000102C1865D.

Athy, L.F., 1930. Density, porosity, and compaction of sedimentary rocks. AAPG Bull. 14 (1), 1–24. https://doi.org/10.1306/3D93289E-16B1-11D7-8645000102C1865D.

Berra, F., Carminati, E., 2012. Differential compaction and early rock fracturing in high-relief carbonate platforms: numerical modelling of a Triassic case study (Esino Limestone, Central Southern Alps, Italy). Basin Res. 24 (5), 598–614. https://doi.org/10.1111/j.1365-2117.2012.00542.x.

Berra, F., Carminati, E., Jadoul, F., Binda, M., 2016. Does compaction-induced subsidence control accommodation space at the top of prograding carbonate platforms? Constraints from the numerical modelling of the Triassic Esino Limestone (Southern Alps, Italy). Mar. Petrol. Geol. 78, 621–635. https://doi.org/10.1016/j.marpetgeo.2016.09.033.

Bertotti, G., 2001. Subsidence, deformation, thermal and mechanical evolution of the Mesozoic South Alpine rifted margin: an analogue for Atlantic-type margins. Spec. Publ. Geol. Soc. Lond. 287 (1), 125–141. https://doi.org/10.1144/GSL.SP.2001.187.01.07.

Beydoun, Z.R., 1986. The petroleum resources of the middle east: a review. J. Petrol. Geol. 9 (1), 5–27. https://doi.org/10.1111/j.1747-5457.1986.

Blendinger, W., Blendinger, E., 1989. Windward-leeward effects on Triassic carbonate bank margin facies of the Dolomites, northern Italy. Sediment. Geol. 64 (1–3), 143–166. https://doi.org/10.1016/0037-0738(89)90089-4.

Boro, H., Bertotti, G., Hardebol, N.J., 2013. Distributed fracturing affecting isolated carbonate platforms, the Latemar platform natural laboratory (Dolomites, North Italy). Mar. Petrol. Geol. 40, 69–84. https://doi.org/10.1016/j.marpetgeo.2012.09.012.

Bosellini, A., 1984. Progradation geometries of carbonate platforms: examples from the Triassic of the Dolomites, northern Italy. Sedimentology 31, 1–24. https://doi.org/10.1111/j.1365-3091.1984.tb00720.x.

Bosellini, A., Neri, C., 1991. The Sella platform. In: Guidebook Excursion B of the Dolomieu Conference on Carbonate Platforms and Dolomitization. Ortisei, Italy.

Bosellini, A., Masetti, D., Neri, C., 1982. La geologia del passo Falzarego. Bologna. In: Castellarin, A., Vai, G.B. (Eds.), a cura di): Guida alla geologia del Sudalpino centro-orientale. Guide geol. reg. S.G.I. 273-278, ISBN 978-8837101916.

Bosellini, A., Gianolla, P., Stefani, M., 2003. Geology of the dolomites. Episodes 26 (3), 181–185. https://doi.org/10.18814/epiiugs/2003/v26i3/005.

Budd, D.A., Frost III, E.L., Huntington, K.W., Allwardt, P.F., 2013. Syndepositional deformation features in high-relief carbonate platforms: long-lived conduits for diagenetic fluids. J. Sediment. Res. 83 (1), 12–36. https://doi.org/10.2110/jsr.2013.3.

Burnham, B.S., Hodgetts, D., 2019. Quantifying spatial and architectural relationships from fluvial outcrops. Geosphere 15 (1), 236–253. https://doi.org/10.1130/GES01574.1.

Caputo, R., 1996. The polyphase tectonics of eastern Dolomites, Italy. Mem. Sci. Geol. 48, 93–106.

Caputo, R., 2008. Polyphase tectonic in the Cortina d'Ampezzo area, eastern Dolomites. Rendiconti Online Società Geologica Italiana 1 (1), 57–63.

Caputo, R., Poli, M.E., Zanferrari, A., 2010. Neogene–Quaternary tectonic stratigraphy of the eastern Southern Alps, NE Italy. J. Struct. Geol. 32 (7), 1009–1027. https://doi.org/10.1016/j.jsg.2010.06.004.

Caputo, R., Stefani, M., Dalpiaz, G., 1999. Contractional and transcurrent tectonics in the Marmolada Group (Dolomites, Italy). Mem. Sci. Geol. 51 (1), 61–63.

Casini, G., Hunt, D.W., Monsen, E., Bounaim, A., 2016. Fracture characterization and modeling from virtual outcrops. AAPG (Am. Assoc. Pet. Geol.) Bull. 100 (1), 41–61. https://doi.org/10.1306/09141514228.

Castellarin, A., Cantelli, L., Fesce, A.M., Mercier, J.L., Picotti, V., Pini, G.A., Prosser, G., Selli, L., 1992. Alpine compressional tectonics in the Southern Alps. Relationships with the N-Apennines. Ann. Tect. 6 (1), 62–94.

Cawood, A.J., Bond, C., Howell, J., Butler, R.W.H., Totake, Y., 2017. LiDAR, UAV or compass-clinometer? Accuracy, coverage and the effects on structural models. J. Struct. Geol. 98, 67–82. https://doi.org/10.1016/j.jsg.2017.04.004.

Corradetti, A., Tavani, S., Parente, M., Iannace, A., Vinci, F., Pirmez, C., Torrieri, S., Giorgioni, M., Pignalosa, A., Mazzoli, S., 2017. Distribution and arrest of vertical through-going joints in a seismic-scale carbonate platform exposure (Sorrento peninsula, Italy): insights from integrating field survey and digital outcrop model. J. Struct. Geol. 108, 121–136. https://doi.org/10.1016/j.jsg.2017.09.009.

Della Porta, G., Kenter, J.A., Bahamonde, J.R., 2004. Depositional facies and stratal geometry of an Upper Carboniferous prograding and aggrading high-relief carbonate platform (Cantabrian Mountains, N Spain). Sedimentology 51 (2), 267–295. https://doi.org/10.1046/j.1365-3091.2003.00621.x.

Doglioni, C., 1987. Tectonic of the dolomites (southern Alps, northern Italy). J. Struct. Geol. 9, 181–193. https://doi.org/10.1016/0191-8141(87)90024-1.

Doglioni, C, Castellarin, A, 1985. A geologic schematic cross-section of the Southern Alps. Rendiconti della Società Geologica Italiana 8, 35–36.

Doglioni, C., Goldhammer, R.K., 1988. Compaction-induced subsidence in the margin of a carbonate platform. Basin Res. 1 (4), 237–246. https://doi.org/10.1111/j.1365-2117.1988.tb00019.x.

Franceschi, M., Preto, N., Caggiati, M., Gattolin, G., Riva, A., Gianolla, P., 2020. Drowning of microbial mounds on the slopes of the Latemar platform (middle Triassic). Italian J. Geosci. 139 (1), 98–108. https://doi.org/10.3301/IJG.2019.23.

Frost III, E.L., Kerans, C., 2009. Platform-margin trajectory as a control on syndepositional fracture patterns, Canning Basin, Western Australia. J. Sediment. Res. 79 (2), 44–55. https://doi.org/10.2110/jsr.2009.014.

Gattolin, G., Preto, N., Breda, A., Franceschi, M., Isotton, M., Gianolla, P., 2015. Sequence stratigraphy after the demise of a high-relief carbonate platform (Carnian of the Dolomites): sea-level and climate disentangled. Palaeogeogr. Palaeoclimatol. Palaeoecol. 423, 1–17. https://doi.org/10.1016/j.palaeo.2015.01.017.

Gianolla, P., Micheletti, C., Panizza, M., Viola, F., 2008. Nomination document. In: Nomination of the Dolomites for Inscription on the World Natural Heritage List UNESCO, vol. 1. Official Dossier, Dolomiti-UNESCO Foundation, Cortina d'Ampezzo, Belluno, p. 1204. Retrieved from. https://whc.unesco.org/uploads/nominations/1237rev.pdf.

Gianolla, P., Caggiati, M., Riva, A., 2021. The interplay of carbonate systems and volcanics: cues from the 3D model of the middle Triassic Sciliar/Schlern platform (dolomites, southern Alps). Mar. Petrol. Geol. 124, 104794. https://doi.org/10.1016/j.marpetgeo.2020.104794.

Goldscheider, N., Mádl-Szőnyi, J., Erőss, A., Schill, E., 2010. Thermal water resources in carbonate rock aquifers. Hydrogeol. J. 18 (6), 1303–1318. https://doi.org/10.1007/s10040-010-0611-3.

Hardebol, N.J., Maier, C., Nick, H., Geiger, S., Bertotti, G., Boro, H., 2015. Multiscale fracture network characterization and impact on flow: a case study on the Latemar carbonate platform. J. Geophys. Res. Solid Earth 120 (12), 8197–8222. https://doi.org/10.1002/2015JB011879.

Hodgetts, D., Drinkwater, N.L., Hodgson, J., Kavanagh, J., Flint, S.S., Keogh, K.J., Howell, J.A., 2004. Three-dimensional geological models from outcrop data using digital data collection techniques: an example from the Tanqua Karoo depocentre, South Africa. Geol. Soc. London Special Pub. 239, 57–75. https://doi.org/10.1144/GSL.SP.2004.239.01.05.

Hunt, D., Fitchen, W.M., 1999. Compaction and the dynamics of carbonate-platform development: insights from the Permian Delaware and Midland basins, Southeast New Mexico and West Texas, USA. Outcrops and Models. In: Advances in Carbonate Sequence Stratigraphy: Application to Reservoirs, vol. 63. SEMPS Special Publication, pp. 75–106. https://doi.org/10.2110/pec.99.11.0075.

Ibrayev, F., Fernandez-Ibanez, F., DeGraff, J.M., 2016. November). Using a genetic-based approach to enhance natural fracture characterization in a giant carbonate field. In: SPE Annual Caspian Technical Conference & Exhibition. OnePetro. https://doi.org/10.2118/182565-MS.

Inama, R., 2021. Fracture analysis and depositional geometries of a high relief carbonate platform from UAV photogrammetry and Digital Outcrop Modeling. The case of the Lastoni di Formin (Italian dolomites) [Doctoral dissertation, Università di Pavia]. IRIS. https://iris.unipv.it/retrieve/handle/11571/1431676/465637/TESI%20DOTTORATO%20RICCARDO%20INAMA.pdf.

Inama, R., Menegoni, N., Perotti, C., 2020. Syndepositional fractures and architecture of the lastoni di formin carbonate platform: insights from virtual outcrop models and field studies. Mar. Petrol. Geol. 121, 104606. https://doi.org/10.1016/j.marpetgeo.2020.104606.

Keim, L., Schlager, W., 1999. Automicrite facies on steep slopes (Triassic, Dolomites, Italy). Facies 41 (1), 15–25. https://doi.org/10.1007/BF02537457.

Keim, L., Schlager, W., 2001. Quantitative compositional analysis of a Triassic carbonate platform (Southern Alps, Italy). Sediment. Geol. 139 (3–4), 261–283. https://doi.org/10.1016/S0037-0738(00)00163-9.

Keim, L., Brandner, R., Krystyn, L., Mette, W., 2001. Termination of carbonate slope progradation: an example from the Carnian of the Dolomites, Northern Italy. Sediment. Geol. 143 (3–4), 303–323. https://doi.org/10.1016/S0037-0738(01)00106-3.

Kenter, J.A.M., 1990. Carbonate platform flanks: slope angle and sediment fabric. Sedimentology 37, 777–794. https://doi.org/10.1111/j.1365-3091.1990.tb01825.x.

Kenter A.M., J, Harris M, P, Della Porta, G, 2005. Steep microbial boundstone-dominated platform margins—examples and implications. Sediment. Geol. 178 (1–2), 5–30. https://doi.org/10.1016/j.sedgeo.2004.12.033.

Koša, E., Hunt, D.W., 2005. Growth of syndepositional faults in carbonate strata: upper Permian Capitan platform, New Mexico, USA. J. Struct. Geol. 27 (6), 1069–1094. https://doi.org/10.1016/j.jsg.2005.02.007.

Leonardi, P., 1968. Le Dolomiti. Geologia dei Monti tra Isarco e Piave. Manfrini, Rovereto, p. 1021.

Marangon, A., Gattolin, G., Della Porta, G., Preto, N., 2011. The Latemar: a flat-topped, steep fronted platform dominated by microbialites and synsedimentary cements. Sediment. Geol. 240 (3–4), 97–114. https://doi.org/10.1016/j.sedgeo.2011.09.001.

Maurer, F., 2000. Growth mode of middle Triassic carbonate platforms in the western Dolomites (Southern Alps, Italy). Sediment. Geol. 134 (3–4), 275–286. https://doi.org/10.1016/S0037-0738(00)00049-X.

Menegoni, N., Meisina, C., Perotti, C., Crozi, M., 2018. Analysis by UAV digital photogrammetry of folds and related fractures in the Monte Antola Flysch formation (Ponte Organasco, Italy). Geosciences 8, 299. https://doi.org/10.3390/geosciences8080299.

Mazzoli, S., Helman, M., 1994. Neogene patterns of relative plate motion for Africa-Europe: some implications for recent central Mediterranean tectonics. Geol. Rundsch. 83, 275–286. https://doi.org/10.1007/978-3-662-38521-0_19.

Menegoni, N., Giordan, D., Perotti, C., Tannant, D.D., 2019. Detection and geometric characterization of rock mass discontinuities using a 3D high-resolution digital outcrop model generated from RPAS imagery–Ormea rock slope. Italy Eng. Geol. 252, 145–163. https://doi.org/10.1016/j.enggeo.2019.02.028.

Mollema, P.N., Antonellini, M., 1999. Development of strike-slip faults in the dolomites of the Sella Group, northern Italy. J. Struct. Geol. 21 (3), 273–292. https://doi.org/10.1016/S0191-8141(98)00121-7.

Nairn, A.E.M., Alsharhan, A.S., 1997. Sedimentary Basins and Petroleum Geology of the Middle East. Elsevier. https://doi.org/10.1016/B978-0-444-82465-3.X5000-1.

Nelson, R., 2001. Geologic Analysis of Naturally Fractured Reservoirs. Elsevier, ISBN 978-0-88415-317-7.

Neri, C., Gianolla, P., Furlanis, S., Caputo, R., Bosellini, A., 2007. Note illustrative della Carta Geologica d'Italia. Foglio Cortina d'Ampezzo 029. Scala 1:50.000. Servizio Geologico d'Italia 200. Retrievable at. https://www.isprambiente.gov.it/Media/carg/note_illustrative/29_CortinaAmpezzo.pdf.

Nolting, A., Zahm, C.K., Kerans, C., Alzayer, Y., 2020. The influence of variable progradation to aggradation ratio and facies partitioning on the development of syndepositional deformation in steep-walled carbonate platforms. Mar. Petrol. Geol. 114, 104171. https://doi.org/10.1016/j.marpetgeo.2019.104171.

Nooitgedacht, C.W., Kleipool, L.M., Andeweg, B., Reolid, J., Betzler, C., Lindhorst, S., Reijmer, J.J., 2018. New insights in the development of syn-depositional fractures in rimmed flat-topped carbonate platforms, Neogene carbonate complexes, Sorbas Basin, SE Spain. Basin Res. 30, 596–612. https://doi.org/10.1111/bre.12239.

Passoni, S., 2020. Geometries and facies of "Lastoni di Formin" Triassic carbonate platform (Dolomites, Italy) (Published master's thesis). Department of Earth and Environmental Sciences, University of Pavia, Pavia, Italy.

Peppa, M.V., Hall, J., Goodyear, J., Mills, J.P., 2019. Photogrammetric assessment and comparison of DJI Phantom 4 pro and Phantom 4 RTK small unmanned aircraft systems. Int. Arch. Photogram. Rem. Sens. Spatial Inf. Sci. https://doi.org/10.5194/isprs-archives-XLII-2-W13-503-2019.

Playton, T.E., Janson, X., Kerans, C., James, N.P., Dalrymple, R.W., 2010. Carbonate slopes, 2010. In: James, N.P., Dalrymple, R.W. (Eds.), Facies Models 4, GEOtext 6. Geological Association of Canada, St. John's, Newfoundland, pp. 449–476 (Canada).

Preto, N., Franceschi, M., Gattolin, G., Massironi, M., Riva, A., Gramigna, P., et al., 2011. The Latemar: a Middle Triassic polygonal fault-block platform controlled by synsedimentary tectonics. Sediment. Geol. 234 (1–4), 1–18. https://doi.org/10.1016/j.sedgeo.2010.10.010.

Preto, N., Gianolla, P., Franceschi, M., Gattolin, G., Riva, A., 2017. Geometry and evolution of Triassic high-relief, isolated microbial platforms in the Dolomites, Italy: the Anisian Latemar and Carnian Sella platforms compared. AAPG (Am. Assoc. Pet. Geol.) Bull. 101 (4), 475–483. https://doi.org/10.1306/011817DIG17026.

Reijmer, J.J., 2021. Marine carbonate factories: review and update. Sedimentology 68 (5), 1729–1796. https://doi.org/10.1111/sed.12878.

Resor, P.G., Flodin, E.A., 2010. Forward modeling synsedimentary deformation associated with a prograding steep-sloped carbonate margin. J. Struct. Geol. 32 (9), 1187–1200. https://doi.org/10.1016/j.jsg.2009.04.015.

Rubey, W.W., Hubbert, M.K., 1959. Role of fluid pressure in mechanics of overthrust faulting: II. Overthrust belt in geosynclinal area of western Wyoming in light of fluid-pressure hypothesis. Geol. Soc. Am. Bull. 70 (2), 167–206. https://doi.org/10.1130/0016-7606(1959)70[167:ROFPIM]2.0.CO, 2.

Rusciadelli, G., Di Simone, S., 2007. Differential compaction as a control on depositional architectures across the Maiella carbonate platform margin (central Apennines, Italy). Sediment. Geol. 196 (1–4), 133–155. https://doi.org/10.1016/j.sedgeo.2006.06.006.

Russo, F., Neri, C., Mastandrea, A., Baracca, A., 1997. The mud mound nature of the cassian platform margins of the dolomites A case history: the cipit boulders from Punta Grohmann (Sasso Piatto massif, northern Italy). Facies 36 (1), 25–36. https://doi.org/10.1007/BF02536875.

Saller, A.H., 1996. Differential compaction and basinward tilting of the prograding Capitan reef complex, Permian, west Texas and southeast New Mexico, USA. Sediment. Geol. 101 (1–2), 21–30. https://doi.org/10.1016/0037-0738(95)00115-8.

Schlager, W., 1993. Accommodation and supply—a dual control on stratigraphic sequences. Sediment. Geol. 86 (1–2), 111–136. https://doi.org/10.1016/0037-0738(93)90136-S.

Schmoker, J.W., Halley, R.B., 1982. Carbonate porosity versus depth: a predictable relation for south Florida. AAPG Bull. 66 (12), 2561–2570. https://doi.org/10.1306/03B5AC73-16D1-11D7-8645000102C1865D.

Schönborn, G., 1999. Balancing cross sections with kinematic constraints: The Dolomites (northern Italy). Tectonics 18 (3), 527–545. https://doi.org/10.1029/1998TC900018.

Sclater, J.G., Christie, P.A., 1980. Continental stretching: an explanation of the post-mid-Cretaceous subsidence of the central North Sea basin. J. Geophys. Res. Solid Earth 85 (B7), 3711–3739. https://doi.org/10.1029/JB085iB07p03711.

Stefani, M., Furin, S., Gianolla, P., 2010. The changing climate framework and depositional dynamics of Triassic carbonate platforms from the Dolomites. Palaeogeogr. Palaeoclimatol. Palaeoecol. 290 (1–4), 43–57. https://doi.org/10.1016/j.palaeo.2010.02.018.

Stott, E., Williams, R.D., Hoey, T.B., 2020. Ground control point distribution for accurate kilometre-scale topographic mapping using an RTK-GNSS unmanned aerial vehicle and SfM photogrammetry. Drones 4 (3), 55. https://doi.org/10.3390/drones4030055.

Štroner, M., Urban, R., Reindl, T., Seidl, J., Brouček, J., 2020. Evaluation of the georeferencing accuracy of a photogrammetric model using a quadrocopter with onboard GNSS RTK. Sensors 20 (8), 2318. https://doi.org/10.3390/s20082318.

Sturzenegger, M., Stead, D., 2009. Close-range terrestrial digital photogrammetry and terrestrial laser scanning for discontinuity characterization on rock cuts. Eng. Geol. 106, 163–182. https://doi.org/10.1016/j.enggeo.2009.03.004.

Taddia, Y., Stecchi, F., Pellegrinelli, A., 2019. Using DJI Phantom 4 RTK drone for topographic mapping OF coastal areas. Int. Arch. Photogram. Rem. Sens. Spatial Inf. Sci. https://doi.org/10.5194/isprs-archives-XLII-2-W13-625-2019.

Taddia, Y., González-García, L., Zambello, E., Pellegrinelli, A., 2020. Quality assessment of photogrammetric models for Façade and building reconstruction using DJI Phantom 4 RTK. Rem. Sens. 12 (19), 3144. https://doi.org/10.3390/rs12193144.

Tavani, S., Corradetti, A., Billi, A., 2016. High precision analysis of an embryonic extensional fault-related fold using 3D orthorectified virtual outcrops: the viewpoint importance in structural geology. J. Struct. Geol. 86, 200–210. https://doi.org/10.1016/j.jsg.2016.03.009.

Thiele, S.T., Grose, L., Samsu, A., Micklethwaite, S., Vollgger, S.A., Cruden, A.R., 2017. Rapid, semi-automatic fracture and contact mapping for point clouds, images and geophysical data. Solid Earth 8, 1241–1253. https://doi.org/10.5194/se-8-1241-2017.

Trombetta, G.L., 2011. Facies analysis, geometry and architecture of a Carnian carbonate platform: the Settsass/Richthofen reef system (Dolomites, Southern Alps, northern Italy). Geo.Alp 8, 56–75.